WIND-TUNNEL STUDY OF WIND LOADS ON PHOTOVOLTAIC STRUCTURES

by

M. Poreh*, J. A. Peterka**

and J. E. Cermak***

for

Bechtel National, Inc.
P.O. Box 3963
San Francisco, California 94119

Fluid Mechanics and Wind Engineering Program
Fluid Dynamics and Diffusion Laboratory
Department of Civil Engineering
Colorado State University
Fort Collins, Colorado 80523

September 1979

* Visiting Professor (from Department of Civil Engineering, Technion, Haifa, Israel)
** Associate Professor
*** Professor-in-Charge, Fluid Mechanics and Wind Engineering Program

CER79-80MP-JAP-JEC12

TABLE OF CONTENTS

TABLE OF CONTENTS

LIST OF FIGURES

LIST OF FIGURES

LIST OF TABLES

1. INTRODUCTION

An important factor influencing the design and subsequently cost of large photovoltaic power generating systems which involve a large number of simple structural elements and supports, is the magnitude of wind-induced loads. This concern was revealed during the course of work performed by Bechtel National Inc. for Sandia Laboratories, Albuquerque, in the Photovoltaics Technology Developments Program funded by the U.S. Department of Energy. The work described in this report was done for Bechtel as part of that national program. It has been recognized by Bechtel that usual design procedures, like the ANSI code (A58.1 - 1972) for example [1], are not adequate for accurate wind design of these repetitive, photovoltaic arrays with their distinctive configuration, orientation and limited height. In fact, the information presently available in the technical literature is not sufficient even for an optimum design of the structure for supporting a single photovoltaic array. Wind Loads on individual arrays at different locations in a large array field are more difficult to determine as they vary according to the array location in the field and wind direction in a complicated manner. Higher loads are expected to exist at the edges of the field, but those might be reduced by carefully designed fences or barriers.

Wind loading is determined by the following groups of factors;

- Magnitude of wind speed.
- The direction of the mean wind relative to the structure.
- The structure of the wind field near the ground; the mean velocity distribution and turbulence. These are primarily determined by the upwind terrain topography and roughness.

- The particular shape and dimensions of the structure and its height above the ground.
- The effect of nearby structures, fences or wind barriers.

Considering these factors, the following wind tunnel testing program has been designed by the authors in collaboration with Bechtel and Sandia, and carried out in the Meteorological Wind Tunnel of the Fluid Dynamics and Diffusion Laboratory, Colorado State University (see Fig. 1):

- Preliminary tests to determine the appropriate model geometrical scaling for adequate simulation of the wind loadings and for examining the possible effect of the Reynolds number on the wind tunnel simulation.
- Wind loading measurements on a single standard photovoltaic array for different wind directions and different angles of attack (see Figs. 2 and 3). These tests were conducted in a boundary layer with a 1/7th power law velocity distribution which characterizes the atmospheric boundary layer over an open flat area.
- Tests in two different boundary layers with different mean velocity and turbulence characteristics.
- A series of tests to evaluate the effect of various design parameters on the wind loadings on a single array. The parameters examined were the panel height (H), see Fig. 3, the aspect ratio of the panel (L/C), the porosity of the panel (P) and the effect of various fences and barriers on the wind loadings. These series of tests were performed at the critical wind directions identified in early phases of the study.

- Tests of wind loading on individual arrays at different locations in an array field, as well as of the effect of various type fences on the arrays located near the edges of the field.

The measurements were accompanied by a flow visualization study, aimed at revealing the nature of the flow field and the aerodynamic characteristics of the photovoltaic arrays, which was recorded in still photographs and a motion picture.

The wind tunnel measurements were analyzed and effects of the various parameters were identified. The results of the analysis are presented in ready-to-use form for calculating the wind loadings on the phototype photovoltaic structures.

2. EXPERIMENTAL CONFIGURATION

2.1 Wind Tunnel

The Meteorological Wind Tunnel of the Fluid Dynamics and Diffusion Laboratory at Colorado State University (Fig. 1) is characterized by a long (96 ft), slightly diverging test section, 6 ft-8 in. wide (at the turntable) and 6 ft high. The ceiling is adjustable to avoid pressure gradient along the test section. This facility is driven by a 400 HP variable pitch propeller with air flow velocity varying continuously from 0.5 fps up to 100 fps. The turntable where the tests were conducted (78 in. diameter) was located near the end of the test section. The ambient temperature was controlled at 24°C.

2.2 Flow Simulation

The primary consideration in modeling wind forces on structures in a wind tunnel is that the wind characteristics in the tunnel simulate natural boundary-layer winds at the actual site. In general, this requires that the vertical distribution of mean velocity and turbulence in the wind-tunnel boundary layer match those at the site and that the Reynolds numbers of the model and the prototype be equal. In addition, the small-scale model must be geometrically similar to its prototype. A detailed discussion of these requirements and their implementation in the wind-tunnel environment can be found in references 2, 3, and 4.

The construction of a 1:24 scale model of a prototype structure and its immediate surroundings (in this case, a flat, open area), submerged in a turbulent boundary layer of the meteorological wind tunnel shown in Figure 1, satisfies all the above criteria except those of equal Reynolds numbers and similarity of turbulence intensity and scale.

In the Reynolds number $\frac{UD}{\nu}$, ν is the same for both the tunnel and the full-scale structure. Because of this, the wind-tunnel air speed, U, would have to be 24 times the full-scale value if the model and prototype Reynolds numbers are to be equal. Testing at such high wind speeds is not feasible. However, for Reynolds numbers larger than 2×10^4 for sharp-edged structures where the flow separation point is fixed, there is no significant change in the values of aerodynamic coefficients as the Reynolds number increases. Since typical Reynolds number values are 10^6-10^7 for high-wind, full-scale flow and about 1×10^5 for wind-tunnel flows, acceptable flow similarity is achieved without equality of Reynolds numbers.

At a model scale of 1:24, the larger scales of turbulence in the atmospheric boundary layer are not simulated in the wind-tunnel flow. However, because the integral scale of the turbulence in the wind tunnel was 2 to 3 times the largest dimension of the model collector, the influence of the scale of turbulence was not expected to be significant (5). Evidence exists which demonstrates some influence of turbulence intensity on drag of flat plates (5,6,7). Because the turbulence intensity difference between the current simulation and a simulation with complete similarity of turbulent structure is not large, the effects due to turbulence intensity should be small. For cases where an upstream collector disturbs the approach flow, turbulence characteristics are dominated by the wake characteristics of the upstream object and possible differences due to turbulence intensity should further decrease.

An important factor which affects the wind loadings is the structure of the atmospheric boundary layer near the ground. The boundary layer which develops over a flat terrain is usually characterized by a 1/7th power law mean velocity distribution. It is impossible to simulate in a wind tunnel the entire atmospheric boundary layer at the desired model scale for this study (1:24). One can, however, simulate the lower part of the atmospheric boundary layer in a 45 in. deep wind tunnel boundary layer [2-4].

The shape of the 1/7th power law boundary layer, which will be referred to as Boundary Layer 1 (BL1) was obtained by means of selected roughness on the wind tunnel floor upstream of the model. Forty ft of test section length were covered with 1 in. cubes followed by a 40 ft length of pegboard with 0.5 in. diameter pegs projecting 0.5 in. above the pegboard base (see Fig. 2). In addition to the floor roughness, four triangular spires were installed at the test section entrance in order to get a thicker boundary layer than would otherwise be obtained. The normalized velocity and turbulence profiles of this boundary layer are shown in Fig. 5a and data is tabulated in Table 1. Turbulence intensity is the root-mean-square of the longitudinal fluctuating velocity divided by the local mean velocity. The turbulence intensity reached values of 20 percent in the boundary layer.

The spectrum of longitudinal velocity fluctuations is shown for BL1 in Fig. 5b including two suggested analytical models of velocity spectra for the atmosphere by Harris (8) and Davenport (9). The spectrum was obtained at 15 inches above the wind tunnel floor. In this plot n is frequency, $F(n)$ is the velocity spectrum, U^2_{rms} is the variance of the fluctuating velocity, δ is the simulated boundary layer height (900 ft full-scale), and U_δ is the velocity at δ. The region where turbulence structure may be important to the determination of loading ranges upward from abscissa values of about 20 for wind speeds up to about 30 mph at 30 ft. Thus, the simulation has a turbulence intensity somewhat too high in the frequency range affecting wind loading on the model and too low in the low-frequency gusts.

Boundary Layer 2 (BL2) was obtained by placing 1 in. cubes along the entire length of the wind tunnel. It is characterized by a 0.24 power law and has a maximum turbulence level of 30% as shown in Fig. 6 and Table 2. Boundary Layer 3 (BL3) is characterized by a 0.19 power law but has an augmented turbulence level with a maximum of 34%. It was obtained by introducing a large disturbance 40 ft upstream the model, followed by the peg roughness of BL1. Its mean velocity and turbulence characteristics are shown in Fig. 6 and tabulated in Table 3.

2.3 The Models

Three brass models of the standard photovoltaic array having geometrical scaling of 1:12, 1:24 and 1:48 were constructed. The standard array was defined by the sponsor to have the following full-scale dimensions: L = 24 ft, C = 8 ft, H = 2 ft, and β = 35 degrees (Figs. 3 and 4). Thus the 1:24 model collector had dimensions of L = 12 in. and C = 4 in. Figure 2 shows the 1:24 model in the wind tunnel. A 1:24 model of a porous array and 1:24 models of arrays with different aspect ratios were also built. Figure 7 shows the different model arrays and their relative size.

Each model could be mounted on a force balance transducer which was connected to the turntable. Figure 8 shows the 1:24 model mounted on the force balance. The turntable indicated the azimuthal angle of the array to an accuracy of 0.2 degrees.

To study the wind loadings on an array located in an array field, 1:24 scale models of array rows were constructed, which could be placed on the wind tunnel floor at desired locations to simulate the relative position in the field of the metric array, on which the wind loading was measured. Figure 9 shows a photograph of a 1:24 model of a photovoltaic array field in the wind tunnel.

3. INSTRUMENTATION AND DATA ACQUISITION

3.1 Measurements of Forces and Moments

Mean force and moment measurements on the instrumented model were made using an Inca six-component strain-gage force balance. The balance was aligned with its axes ($\bar{x}$, $\bar{y}$, $\bar{z}$) parallel to the x, y and z coordinate system fixed to the model, as shown in Figs. 3, 4, and 9. Two forces and three moments were measured on the model in this project as the FZ transducer could not measure the small forces in the direction along the array support.

Each strain-gage bridge of the balance was monitored by a Honeywell Accudata 118 Gage Control/Amplifier unit which provided excitation to the bridge and amplified the bridge output. These instruments are characterized by a stable excitation voltage and amplifier gain. Each channel signal was further processed through a low-pass filter and then fed by means of analog lines specially designed to minimize distortion to a Preston Model GMAD-4 analog-to-digital converter. The transducer outputs were recorded simultaneously for 60 seconds at a 100 sample per second rate. The data was then analyzed by a Hewlett-Packard System 1000 minicomputer under program control and recorded. The minicomputer calculated the moments MX, MY, MZ in the x, y, z coordinate system, using the values of the distances XBC, YBC, ZBC, between the original center of moments of the balance (B) and the center (C) of the coordinate system x, y, x (see Fig. 3). Since FZ could not be measured, the values of MX and MY could not be accurately calculated. Since these moments are not significant parameters in the design of this particular structure, no effort was made to correct them and they are not presented in the report.

Calibration of the balance was performed in a test rig in which known forces and moments could be applied to the balance. A calibration matrix was then obtained for reducing the mean output of the strain gages. The load and strain relationship is linear in the range of loads applied in this study.

Although the calibration matrix was found to be stable, frequent checks of the system were made during the testing program by placing a known weight eccentrically on the model and comparing the system's response with the applied FX, MZ and MX moments.

Since the resultant force acting on the array

$$F_{res} = (FX^2 + FY^2)^{1/2} \tag{1}$$

is expected to be approximately normal to the array surface, as confirmed later in the experiments, the value of F_{res} and of the normal force N, defined as

$$N = FX \sin\beta - FY \cos\beta \ , \tag{2}$$

were compared after each run as an additional check of the system. Note that a positive FN designates a normal force acting toward the surface (see Fig. 10).

The force balance and electronic system are supported by their manufactured specifications to be accurate to within 0.1 percent of full-scale (50 lbs). This would indicate a maximum possible error of 5 percent in the force and moment measurements (about 0.015 in force coefficient and 0.01 in moment coefficient), in the 1:24 models for the critical loadings. The maximum possible error in the 1:12 model is expected to be about four times smaller, whereas the errors in the 1:48 model could be four times larger in the force measurements and eight times larger in the moments measurements. The data shows, however, a very good agreement between the measurements in the 1:24 and 1:12 models, suggesting that the errors are smaller. The scatter in the 1:48 model data, on the other hand, was very large, particularly in the moments measurements, and the 1:48 model data were not used in the analysis. The measured loadings on the metric array in some of the array field tests were also very small and are therefore less accurate than the measurements of the higher loads.

Note that the existing force and moment measurements are average values and do not contain gust loading. Thus, the peak forces and moments for gust loading must be obtained by using a quasi-static loading assumption and an estimated gust velocity. This study did not attempt to determine response.

3.2 Measurements of Flow Characteristics

Velocity and turbulence intensity profiles for the approach flow under test conditions were made at the location of the model in the tunnel (turntable) with the model removed.

The measurements were made with a Thermosystems Model 1050 constant-temperature anemometer with a 0.001 in. diameter platinum film sensing element 0.02 in. long. The sensing probe was attached to a vertical traverse to measure velocities and turbulent intensities at different heights. Output was processed through the same on-line digital data acquisition system described above.

Tests were made at only one wind speed in the tunnel around 90 ft/sec. This wind was sufficiently high to ensure Reynolds number similarity between the model and prototype as will be shown later.

The reference velocity at each test was measured using a pitot tube which was connected to a Setra differential pressure transducer. The pitot tube was placed outside the simulated boundary layer and recorded the value of $q_\infty = \rho U_\infty^2/2$, where ρ is the mass density of the air. The ratio of the reference velocity U_{REF}, at a prototype height of 30 ft above the ground, to U_∞ was determined from the velocity distribution of the boundary layer according to the scale of the model. The value

$$q_{REF} = \frac{\rho U_{REF}^2}{2} = \frac{\rho U_\infty^2}{2} \left(\frac{U_{REF}}{U_\infty}\right)^2 \tag{3}$$

at the height corresponding to 30 ft above ground in the prototype was later used in calculating the dimensionless force and moment coefficients of the array, so that it was not necessary to measure the density of the air.

3.3 Force and Moment Coefficients

It has been established [1-3] that the dimensionless aerodynamic coefficients are the same for the model and prototype, provided the Reynolds numbers of the flows are sufficiently large. Forces and moments on arrays measured in the experiments were therefore converted directly into the dimensionless coefficients defined below:

The drag coefficient

$$CFX = \frac{FX}{q_{REF} \cdot A}, \tag{4}$$

The lift coefficient

$$CFY = \frac{FY}{q_{REF} \cdot A} \tag{5}$$

the normal force coefficient

$$CN = \frac{N}{q_{REF} \cdot A} = CFX \sin\beta - CFY \cos\beta \tag{6}$$

and the pitching moment coefficient

$$CMZ = \frac{MZ}{q_{REF} \cdot A \cdot DXY} \tag{7}$$

where q_{REF} is the reference dynamic pressure at 30 ft above the ground in the prototype as defined in Eq. (3), A is the area of the array (192 sq ft in the prototype of the standard array) and DXY = C/2 is half the chord length of the array (4 ft in the prototype of the standard array), as shown in Figs. 3 and 4.

The displacement distance ε of the normal force N from the center of the array (Fig. 10) can be calculated by the equation

$$\varepsilon = -CMZ/CN.$$

The values of the measured dimensionless coefficients are presented in figures and tabulated at the end of the report.

4. ANALYSIS OF THE EXPERIMENTAL RESULTS

4.1 Reynolds Number Independence Tests

The aerodynamic coefficients measured with the standard array 1:24 scale model (β = 35°) for five reference velocities ranging from 20 ft/sec to 96 ft/sec are plotted as a function of the Reynolds number ($RE = UC/\nu$) in Fig. 11. Obviously, the values of the coefficients measured in the range $Re > 10^5$ (above 50 ft/sec) are independent of the velocity and can thus be used to predict prototype loadings.

The observed scatter of the data below $Re = 10^5$ is probably due to the experimental error which is inversely proportional to the square of the wind speed.

All the tests were therefore conducted using wind tunnel speeds around 90 ft/sec, which correspond to Reynolds numbers around 2×10^5.

The test matrix for forces and moments on a single collector are summarized in Table 4. The various elements of this test series are discussed in Sections 4.2 - 4.8.

4.2 Comparative Tests with Different Model Scalings

The aerodynamic coefficients of the standard array (H = 2 ft, C = 8 ft and L/C = 3) were measured in BL1 with the 1:24 and 1:12 scale models for different angles of attack (β) and wind directions (α). The data which are presented in Figs. 12-14, show an excellent agreement between the values of the coefficients measured with these models and also indicate that the effect of blockage (less than 3 percent in the large model) is negligible.

The 1:12 scale is, however, too large for studying the effect of the fence and the interaction between adjacent models in an array field. It was therefore decided to continue the rest of the tests with the 1:24 model.

The 1:48 array model, on the other hand, was found to be too small as the aerodynamic forces and moments acting on it could not be accurately measured with the force balance, see Fig. 15.

4.3 The Wind Loadings on a Single Standard Array

A rectangular 8 ft x 24 ft array placed above the ground so that H is 2 ft (for any angle of attack β) is defined in this study as a standard array, see Fig. 3.

Figures 12-14 show the measured drag coefficients CFX, lift coefficients CFY, the normal force coefficients CN and the pitching moment coefficients CMZ for $\beta = 25°$, $35°$ and $45°$.

Note that the array axis is in the east-west direction and that its upper surface is tilted toward the south. According to our definition, drag forces FX acting toward the north, lift forces FY acting upward, and normal forces N acting toward the active surface of the photovoltaic array are defined as positive forces. Thus, for $\beta = 25° - 45°$, northerly winds ($\alpha = 0$) give negative drag forces, positive lift forces and negative normal forces, as demonstrated in Fig. 10a which also gives the recorded coefficients for $\beta = 35°$. Southerly winds give positive drag forces, negative lift forces and positive normal forces, as shown in Fig. 10b.

The moments for both wind directions are positive. Defining the relative eccentricity as

$$\bar{\varepsilon} = \frac{\varepsilon}{(C/2)} = - \frac{CMZ}{CN} \qquad (8)$$

one finds that $\bar{\varepsilon}$ is of the order of 0.15, indicating that the shift of the normal force is about 0.15 (C/2) namely 0.6 ft from the center of the prototype array. The eccentricity can be easily calculated from the data tabulated at the end of the report, however, large errors are possible when CN is very small.

In general, the resultant force acting on the array in the x, y plane satisfies the relation

$$F_{res}^2 = FX^2 + FY^2 = N^2 + FT^2 \tag{9}$$

where FT is the force tangent to the active surface of the photovoltaic array. The tangential force should, however, be very small, since the array is almost a flat plate. Indeed, one finds, for $\beta = 35°$ and wind direction $\alpha = 0$, that

$$\begin{aligned} CFT &= CFX \cos\beta + CFY \sin\beta \\ &= -0.44 \cos 35° + 0.60 \sin 35° = -0.02 \end{aligned} \tag{10}$$

which is negligible relative to CN = -0.75. Thus one may conclude that

$$N \cong F_{res} . \tag{11}$$

This important observation indicates that the three aerodynamic coefficients are related and when the value of one of them is known, one can estimate the other two. For example, for a given N

$$FX \cong N \cdot \cos \beta \tag{12}$$

$$FY \cong N \cdot \sin \beta \tag{13}$$

These approximate relations would not hold, of course, as β approaches 0 and significant deviation might occur when the measured forces are small.

The dependence of the aerodynamic coefficients on the wind direction, for the three angles of attack $\beta = 25°$, $35°$, and $45°$, shown in Figs. 12 to 14 appear to be similar. The normal force coefficient is negative at wind direction $\alpha = 0°$. Its absolute value increases slightly when the wind has a westerly or an easterly component and reaches a maximum around $\alpha = 30° - 45°$. It decreases to zero at $\alpha = 90°$ and reaches a peak at $\alpha = 180°$, smaller than its maximum absolute value. The drag and lift coefficients' dependence on the wind direction is approximately the same, except that the lift coefficient has an opposite sign. Note that the curves of lift and drag coefficients for $\beta = 45°$ shown in Fig. 14 appear to be a reflection of each other, as predicted by Eqs. 12 and 13.

The effect of angle β on the aerodynamic coefficients is shown in Figs. 16-18 for three different approach wind directions. Most coefficients are not highly sensitive to variations in β although CFX tends to increase in absolute value monotonically with increasing β as expected and CFY tends to have a weak maxima in absolute value near $\beta = 35°$.

The pitching moment coefficients appear to be positive for all wind directions at most values of β. However, their values are very small and it is quite possible that some negative moments exist for $90° < \alpha < 270°$, as in arrays with $\beta = 75°$ and $\beta = 90°$, see Fig. 18.

It is interesting to compare the values of the drag coefficients for arrays having $\beta = 90°$ at $\alpha = 0°$ and $\alpha = 180°$ with the design coefficient proposed by the Australian Standard for low walls and hoardings [10]. The drag coefficient of the Australian code, based on the reference pressure at H + C (10 ft above the ground in our case) is $C_D = 1.2$. Using a reference velocity at 30 ft in a 0.14 power law boundary layer the coefficient would be

$$C_D = 1.2 \left(\frac{10}{30}\right)^{(2.0)\ (0.14)} = 0.88 \tag{14}$$

which is slightly above the values of CFX = 0.72 for $\alpha = 180°$ measured in the present tests.

4.4 The Effect of the Array Height above the Ground

Figure 19 compares the values of the aerodynamic coefficients of the 8 ft x 24 ft array installed at two elevations above the ground: H = 2 ft and H = 4 ft. It is seen that the force coefficients increase in their absolute value when H is increased to 4 ft. The maximum value of |CN| is increased by approximately 20%. It is interesting to note that the value of |CN| at $\alpha = 45°$ has increased by only 13% because of the shift in the position of the peak. The values of |CN| for $\alpha = 0°$ and $\alpha = 45°$ are plotted versus H in Fig. 20a. The increase of |CN| with H appears to be a mild one. One should recall, however, that H is not related directly to the typical velocities acting on the array. A more representative height is that of the center of the array, namely $H + C \sin\beta/2$. Plotting the various values of |CN| versus $H + C\sin\beta/2$, Fig. 20b, one finds that for $\alpha = 0°$

$$|CN|_{\alpha = 0} \cong (H + C\sin\beta/2)^{0.28} \tag{15}$$

namely

$$|CN|_{a = 0} \cong |U^2| \ (H + C\sin\beta/2). \tag{16}$$

The same law does not describe, however, the change of |CN| at $\alpha = 45°$ probably because the normal force acts at a point above the center of the array and also because the position of the peak of $|CN|$, which occurs around this wind direction, is also changing with H. Nevertheless, it appears from Fig. 20b that Eq. 16 can probably be used for a very rough estimate of the effect of H for other wind directions and boundary layers.

4.5 The Effect of the Porosity of the Array

Tests with different porous arrays (P = 2.5%, 5% and 10%) indicated the effects of the plate porosity is not large. Figure 21 compares the aerodynamic coefficients for the standard impermeable array and a porous plate with P = 10 percent. A small decrease in the values of $|CN|$ particularly for $30° \leq \alpha \leq 60°$ and $120° < \alpha < 150°$ is noticed and one finds that the peak value of $|CN|$ decreased by approximately 10 percent.

4.6 The Effect of Aspect Ratio

Comparison of the measurements of the aerodynamic coefficients measured with arrays with three aspect ratios (AR = 2, 3 and 4), presented in Fig. 22, do not show a clear trend as to the effect of the aspect ratios in this range.

4.7 The Effect of an Upstream Fence

A series of tests have been conducted to examine the effect of an upstream fence or a wind barrier (fence porosity zero) on the aerodynamic forces acting on an individual array. The results of the tests are shown in Figs. 23 and 24.

Figure 23 shows the effect of a 30% porosity fence on the absolute value of CN. The broken lines show the values measured with a 30% porosity fence located 20 ft from the center of the array. A large reduction of $|CN|$ is caused for $\alpha = 0°$ even by a 4 ft fence. When the wind is not perpendicular to the fence, as in the case of $\alpha = 45°$, the fence effectiveness is decreased. The measurements with a porous array (P = 5%) are also shown in this figure. The additional reduction of the normal force due to the array's porosity is very small as already observed in Section 4.5.

The measurements with a 5 ft fence located at different distances from the center of the array are also shown in Fig. 23 for both wind directions. It appears that the distance of the fence is not a critical factor for $\alpha = 0°$ whereas in the case of $\alpha = 45°$, the effect of a fence diminished completely beyond a distance of 8 fence heights.

The effect of the fence porosity is shown in Fig. 24. Decreasing the fence porosity beyond 30% does not affect the value of CN for $\alpha = 45°$. When the wind is perpendicular to the fence, however, the magnitude of CN continues to decrease with the fence porosity until the fence becomes a solid wall (P = 0). It is interesting to note that when P = 0, the direction of CN is reversed indicating that the array is located in a weak vortex behind the solid wall. The presence of such a vortex was confirmed in the flow visualization study.

The values of CMZ reported above should be used with some caution. Because the center of pressure of the mean force N is near the panel centerline, CMZ values are generally small. Fluctuating values of CMZ may be substantially higher.

4.8 The Aerodynamic Coefficients in Different Boundary Layers

The aerodynamic coefficients of the single standard array have been measured in two additional boundary layers (BL2 and BL3) having different power laws 0.26 and 0.20 versus the 0.14 power law of BL1. The turbulence level in BL3 was higher than that in the other boundary layers as discussed earlier.

The primary effect of the power law on the force coefficients is expected to be due to the different ratios of the local velocities at the height of the array for the same velocity at the reference height of 30 ft. Representing the reference height of the array by $H + C\sin\beta/2$ (4.29 ft) one would expect that the ratio of the force coefficients for two boundary layers with n_1 and n_2 power laws would be roughly equal to

$$\frac{CF(n_1)}{CF(n_2)} = \left(\frac{4.29}{30}\right)^{2(n_1 - n_2)}$$

Such a law would predict ratios of CN(0.26)/CN(0.14) = 0.63 and CN(0.20)/CN(0.14) = 0.79.

The values of CN of the single array in the three boundary layers are compared in Fig. 25. Indeed, one finds a reduction of the normal force coefficients in both cases. At some wind directions the reductions are close to that predicted by the above equation. For example CN(0.26)/CN(0.14) was found to be exactly 0.63 for $\alpha = 0$ and was equal to 0.70 at $\alpha = 180°$. On the other hand the force coefficients ratio in BL3 CN(0.20)/CN(0.14) measured at $\alpha = 0°$ and $\alpha = 45°$ were 0.73 and 0.59 respectively, in other words, smaller than the predicted value of 0.79, in spite of the higher level of turbulence.

The only conclusion one can thus draw from these tests is that a reduction in the value of the aerodynamic coefficients in boundary layers with power law velocity exponents greater than the 0.14 power law is expected but its exact magnitude has to be determined experimentally for each use.

4.9 The Array Field Study

4.9.1 Description of the Tests

Two sections of a large array field were studied: the north-eastern corner of the field and its response to winds with northern and eastern components and the south-western corner of the field and its response to winds with southern and western components. The arrays were inclined toward the south with $\beta = 35°$ so that the two sections had different characteristics. A schematic description of the field and the notation used to describe the array field tests are shown in Fig. 26. Figure 9 shows a model of the array field in the wind tunnel.

Models of a porous fence (FP = 30%) and of a solid wall (FP = 0) were built around the field in some of the tests at a distance of LP = 20 ft (see Fig. 26). The effect of an additional diagonal fence in the corner of the field was also investigated in testing the wind loadings on arrays close to the corner, as shown in Fig. 26.

In order to determine the influence of access roadways in the array field, forces and moments were measured on arrays NE7, NE8, SW7 and SW8 with row 6 removed and with rows 8 and 9 removed. Test results with row 6 removed are designated by "x" while test results with rows 8 and 9 removed are designated "xx".

The test matrix for the array field study is shown in Table 5 and the results are discussed in the next section.

4.9.2 Analysis of the Results

The measured aerodynamic coefficients of the different arrays are tabulated in Appendix A at the end of the report. Figures 27-30 show the values of the normal force coefficients measured for each array for different wind directions and fence configurations. The figures also show the values of CN for a single array (without a fence) at each wind direction.

Figure 27 summarizes the measured values of CN for the corner arrays NE1 and SW1. The force coefficients of these corner arrays, without the protection of a fence, are equal or even higher than the corresponding coefficients of a single array. The reason for the increase in the value of CN due to winds normal and almost normal to the arrays is not clear to the authors. The effect of the fence on the wind loading for these wind directions is to reduce their values to approximately 20% of the values for the unprotected arrays. An even larger reduction was achieved by the solid wall. In fact, the solid wall has reversed the direction of the forces acting on the NE1 array for these wind directions, probably because the array is located in the separated flow region where a vortex flow is created. The existence of this vortex was confirmed in the flow visualization study. A reversal in the direction of the force was also found in the case of a single array (see Fig. 24). The reported values of these small forces should, however, be considered only as a rough estimate, since the possible error in measuring such small loads could be relatively high.

The fence is less effective in reducing the loadings due to cornering winds. The solid wall was not very effective in these cases either. In fact it did not reduce at all the loadings on the SW1 array for $\alpha = 225°$. The additional diagonal corner fence was, however, very effective and reduced further the loads on the corner arrays.

Similar effects were observed in testing the NE2 and the SW2 arrays. Their loadings due to normal winds are drastically reduced by either the fence or the solid wall but neither were effective in reducing the loadings due to cornering winds. Adding a corner fence was beneficial, although it did not give these arrays as much protection as it gave NE1 and SW1 arrays. Similar results were obtained for NE5 and the SW5 arrays (see Fig. 28) and the NE7 and SW7 arrays (see Fig. 30).

The normal force coefficients of the unprotected NE2 and SE2 arrays were found to be lower than the corresponding coefficients of the single array. A large reduction is observed due to the porous fence particularly on the SW2 loadings. However, the effect of the solid wall on these arrays was to create relatively large forces in the opposite direction.

The inner arrays NE4 and particularly SW4 (see Fig. 29) were quite protected by the upwind rows. So were the NE6 and NE8, SW6 and SW8; however, the effect of the fence is decreased with distance into array field and higher values of CN are recorded in the NE8 and SW8 arrays (see Fig. 30). It appears from the data that in general the effectiveness of the solid wall in reducing the wind loadings was not as large as that of the porous fence with the additional diagonal corner fences.

In Fig. 31 the maximum values of both the normal force coefficients and the moment coefficients are given for an array field surrounded by a fence and with additional diagonal fences at the corners. The largest values of |CN| are those recorded at the eastern side for north-easterly winds.

The effect of missing rows in the center of the field is shown on the left hand side of Fig. 30. Surprisingly the effect of missing row (NE8X and SW8X), was more drastic than that of two missing rows (NE8XX and SW8XX).

The moment coefficients in the field surrounded by fences were also much smaller than for the single array, reaching a maximum of |CMZ| = 0.06 for the field versus |CMZ| = 0.22 for the isolated array.

5. CONCLUSIONS

The wind loadings on photovoltaic arrays were measured on 1:24 and 1:12 scale wind tunnel models. The dimensionless coefficients measured were independent of the Reynolds number and can therefore be used for the design of prototype arrays. The measured aerodynamic coefficients were independent of scale of model used.

The lift and drag coefficients of the arrays were shown to be related to the normal force coefficients so that only the values of CN and CMZ, the normal force and pitching moment coefficients, are required for the design of the structural supports of the arrays.

The effects of changing the configuration of the standard array have been studied. It appears that neither the height above the ground nor the porosity of the array has a large effect on the aerodynamic coefficient. The effect of changing the array aspect ratio was not large. On the other hand the reduction of the wind loadings on either individual arrays or on an array field by porous fences was very large. A 30% porosity fence with additional corner fence reduces the maximum value of the normal force coefficient from $|CN| = 0.81$ to $|CN| = 0.33$ at the edges of the field and to 0.27 in the center of the field.

REFERENCES

1. American National Standards Institute, American National Standard Building Code Requirements for Minimum Design Loads in Buildings and Other Structures, ANSI Standard A58.1, 1972.

2. Cermak, J. E., Aerodynamics of Buildings, Annual Review of Fluid Mechanics, Vol. 8, 1976.

3. Cermak, J. E., Laboratory Simulation of the Atmospheric Boundary Layer, AIAA Jl., Vol. 9, September 1971.

4. Cermak, J. E., Applications of Fluid Mechanics to Wind Engineering, A Freeman Scholar Lecture, ASME Jl. of Fluids Engineering, Vol. 97, No. 1, March 1975.

5. Bearman, P. W., Turbulence Effects on Bluff Body Mean Flow, Third U.S. National Conference on Wind Engineering Research, pp. 265-272, 1978.

6. Bearman, P. W., An Investigation of the Forces on Flat Plates Normal to a Turbulent Flow, Jl. Fluid Mechanics, Vol. 46, pp. 177-198, 1971.

7. Nakamura, Y. and Tomonari, Y., The Effect of Turbulence on the Drag of Rectangular Prisms, Transactions Japan Society of Aeronautical and Space Science, Vol. 19, pp. 81-86, 1976.

8. Harris, R. I., The Nature of the Wind, Modern Design of Wind Sensitive Structures, Paper 3, 1971.

9. Davenport, A. G., The Spectrum of Horizontal Gustiness Near the Ground, Quarterly Jl., Royal Meteorological Society, V81, pp. 194-211, 1961.

10. Australian Standards. Rules for Minimum Design Loads on Structures (SAA Loading Code) Part 2 - Wind Forces. The Standards Association of Australia, North Sydney, p. 29, 1975.

FIGURES

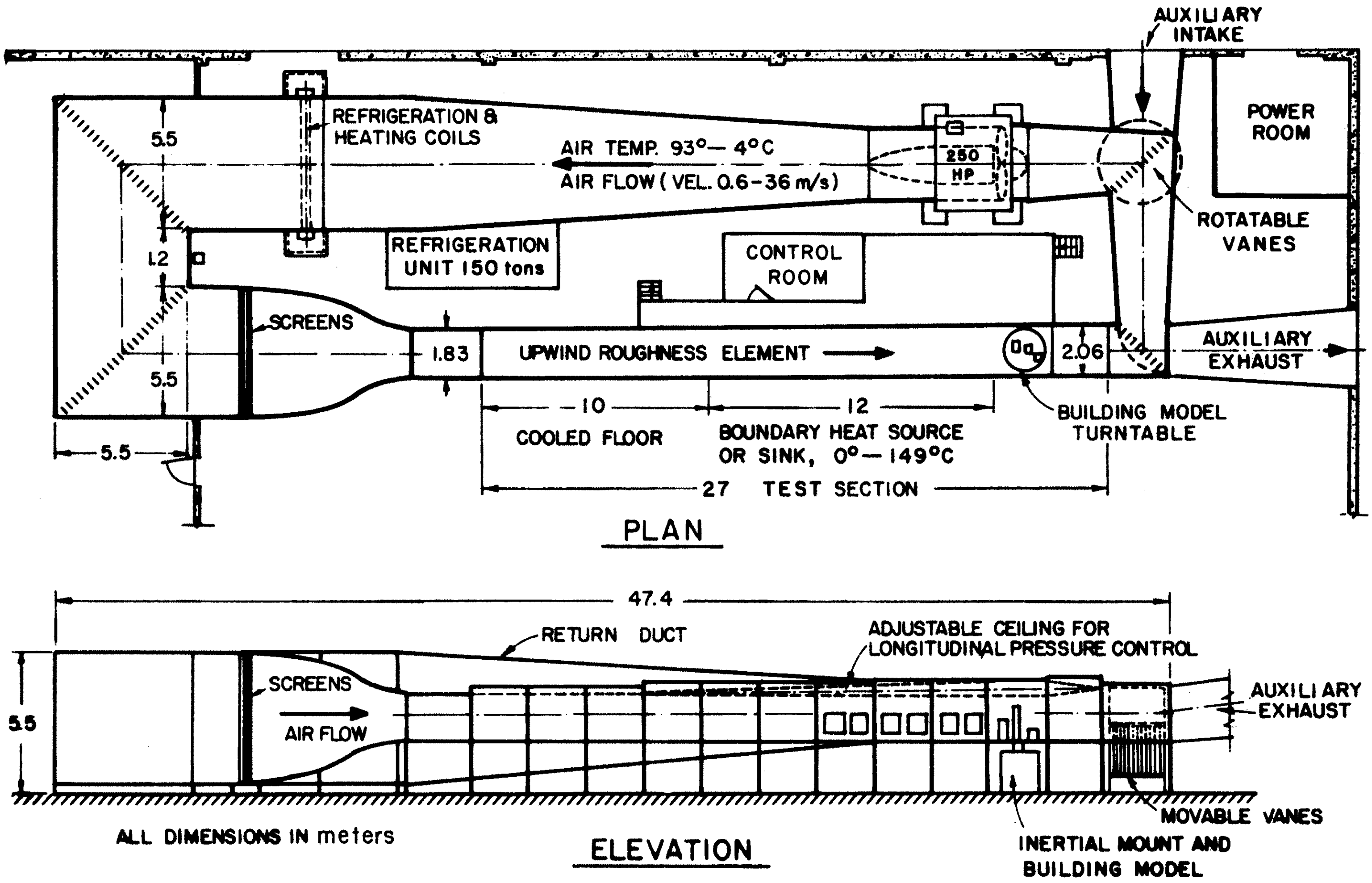

Figure 1. Meterological Wind Tunnel

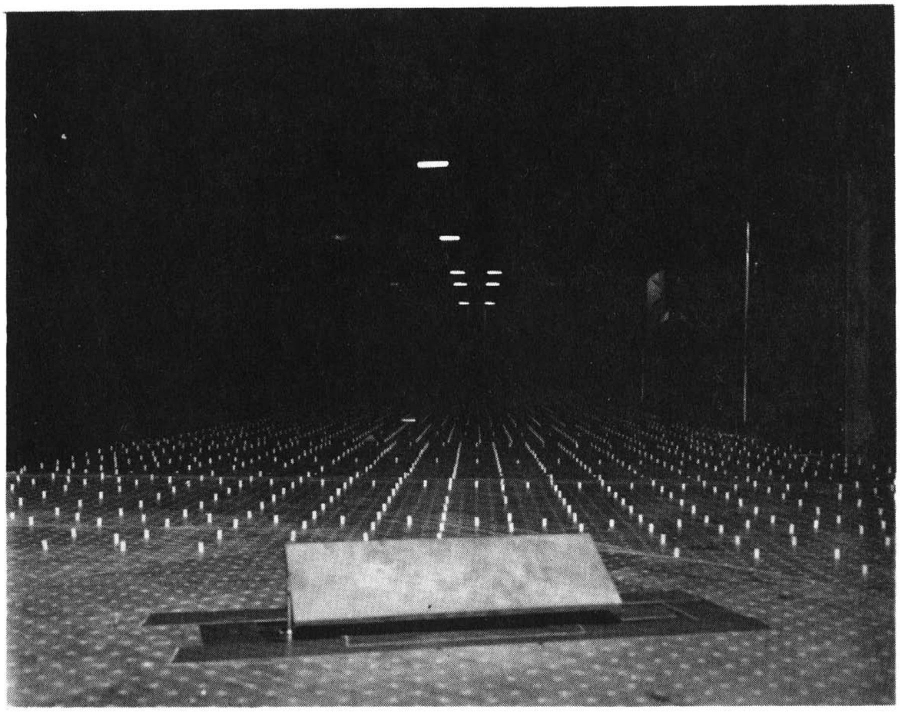

Figure 2. A 1:24 Model of a Single Standard Photovoltaic Array in the Wind Tunnel (Peg Roughness on Boundary Layer 1 is Seen in the Foreground)

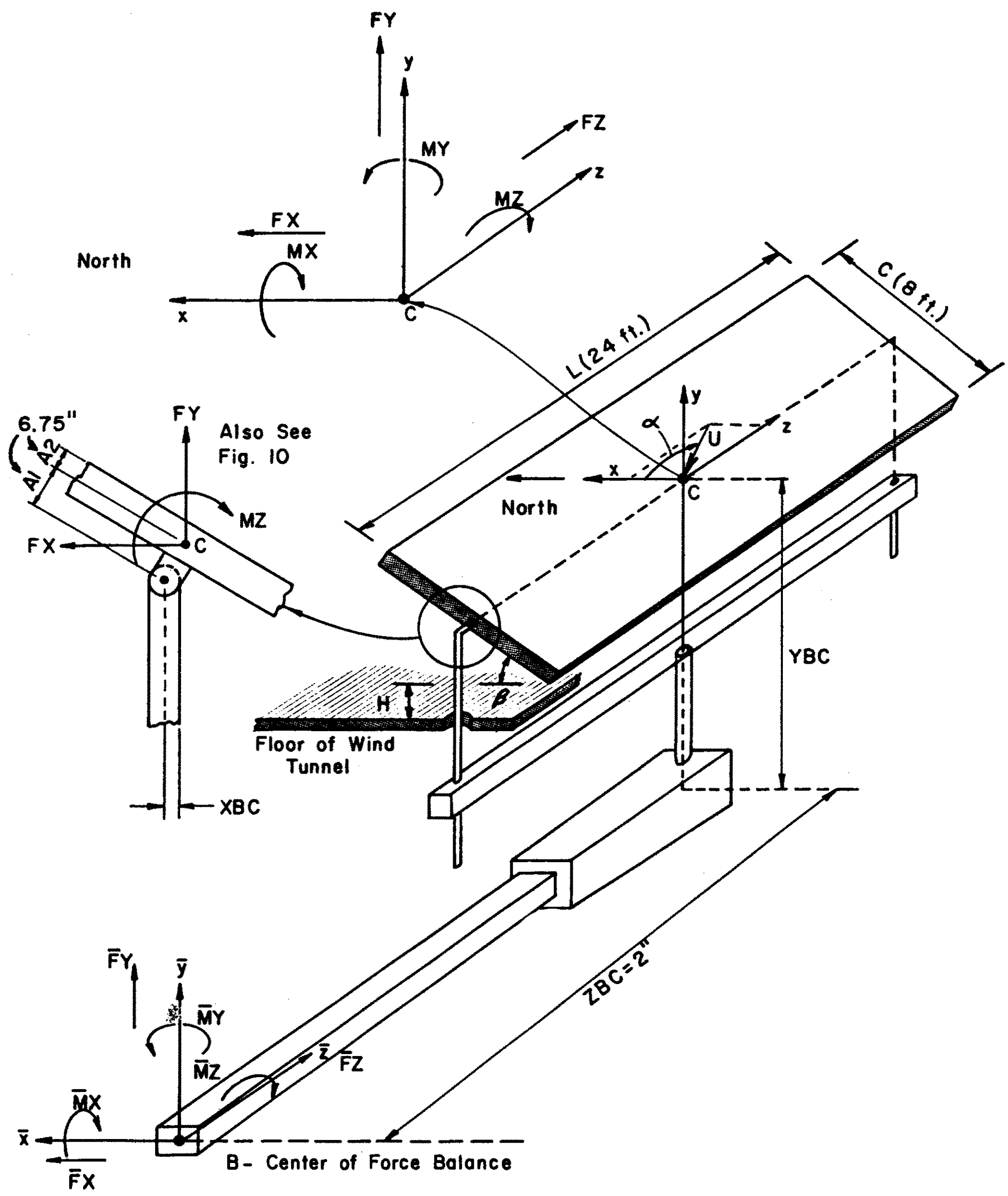

Figure 3. A Schematic Description of a Single Array Model in the Wind Tunnel and the Coordinate System

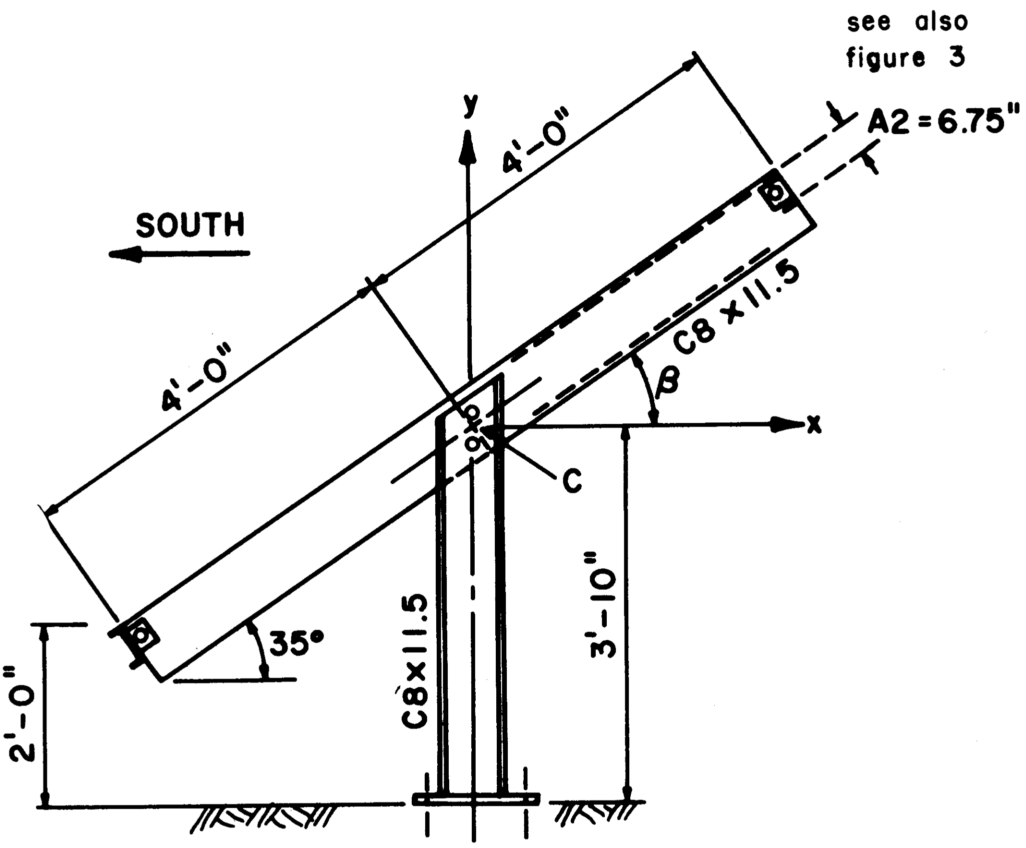

Figure 4. Conceptual Low-Cost Support for a Photovoltaic Array

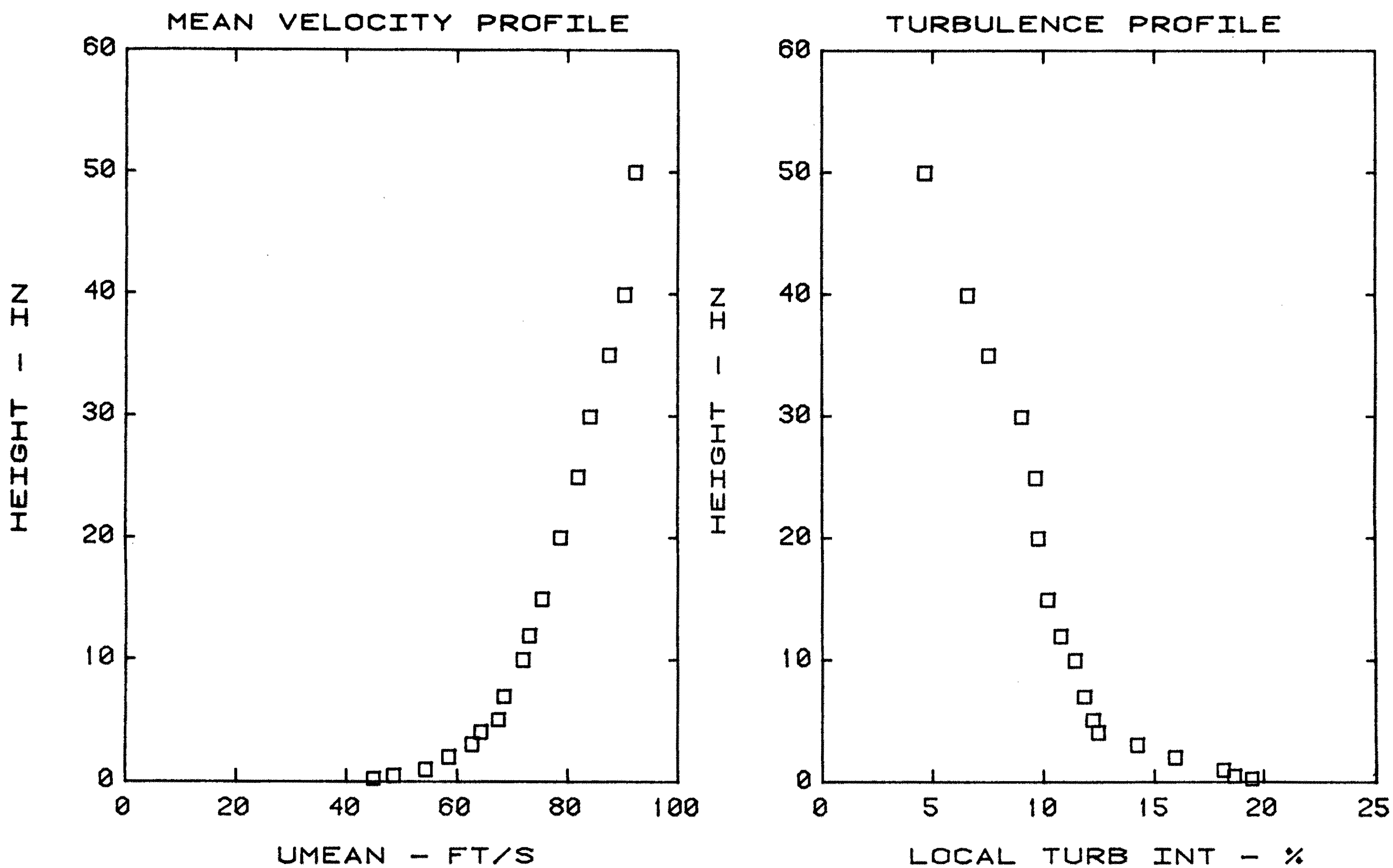

Figure 5a. Mean Velocity and Turbulence Distribution in Boundary Layer 1

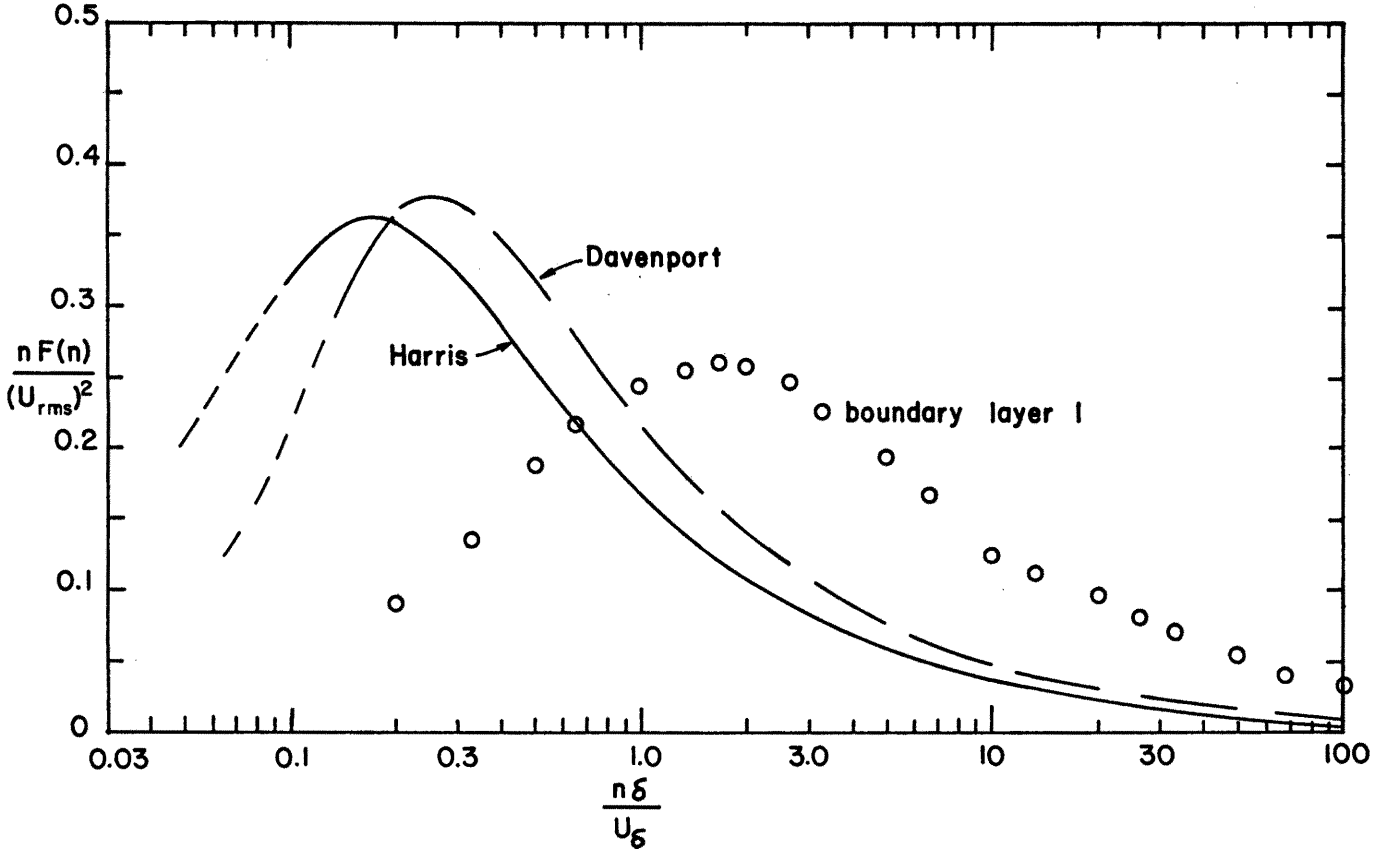

Figure 5b. Turbulence Spectrum in Boundary Layer 1

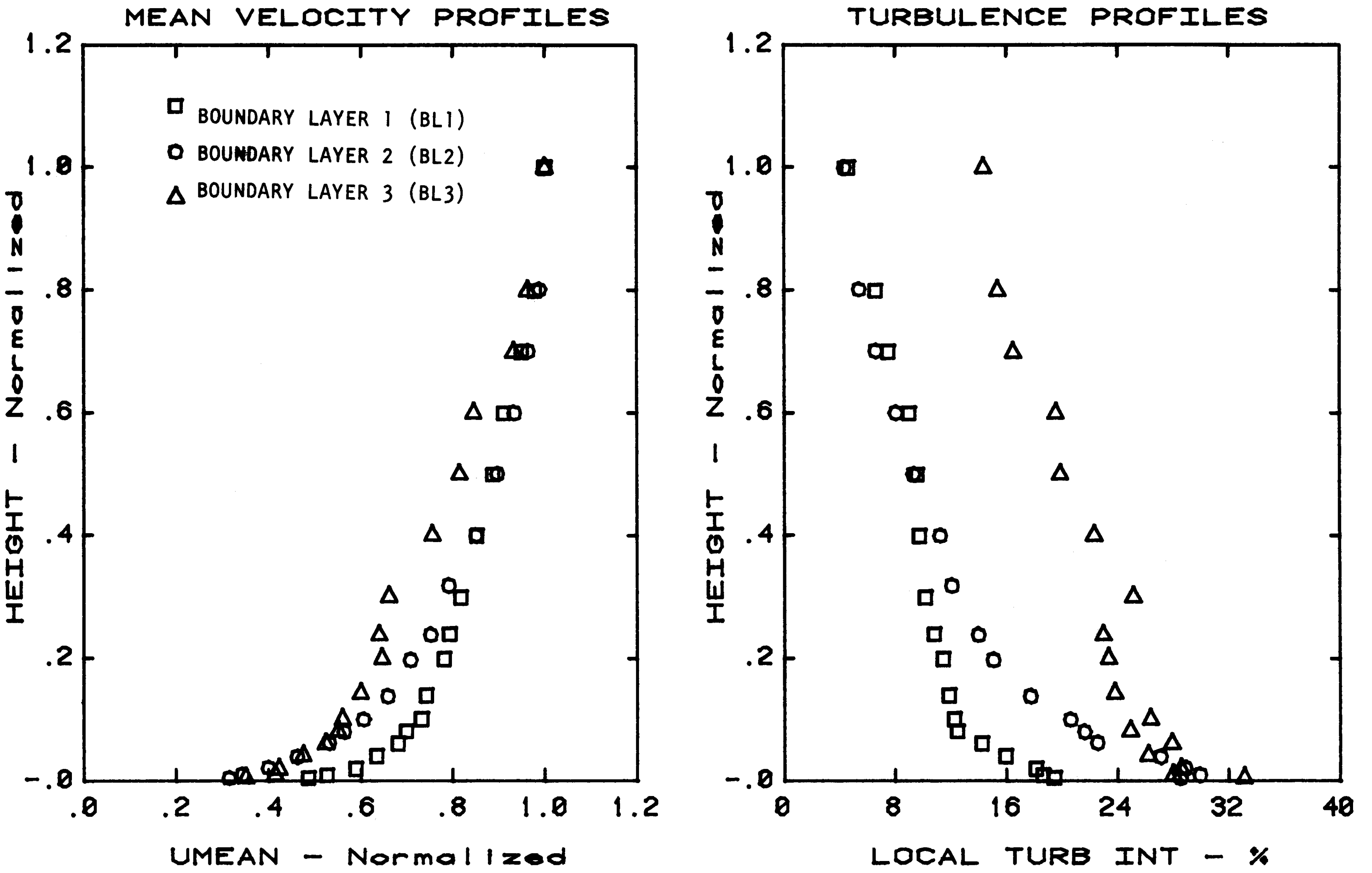

Figure 6. Comparison of Mean Velocity and Turbulence Distribution in Boundary Layers 1, 2 and 3

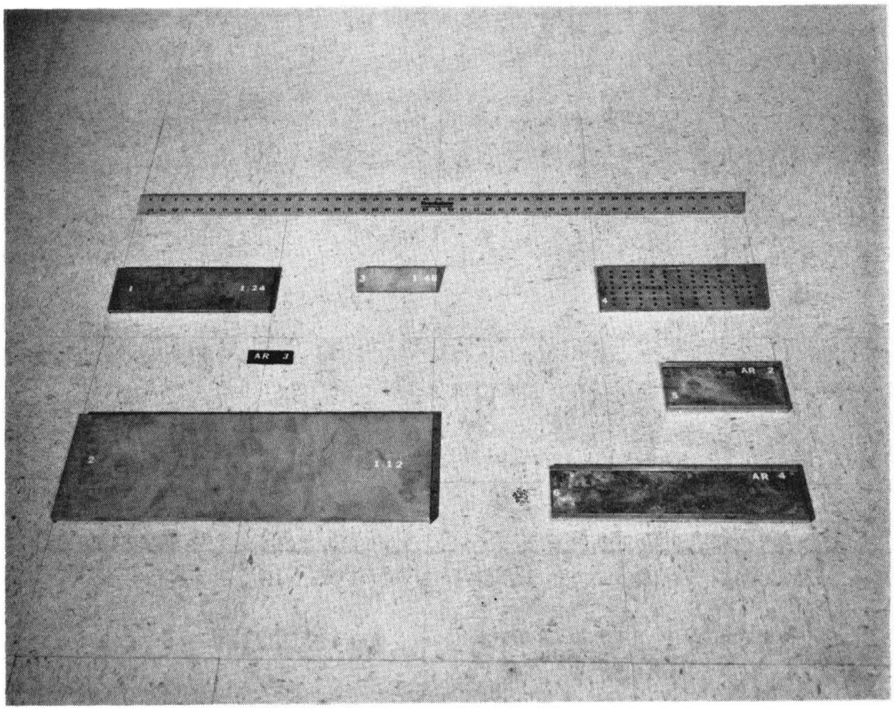

(1) 1:24 standard array, aspect ratio = 3

(2) 1:12 standard array, aspect ratio = 3

(3) 1:48 standard array, aspect ratio = 3

(4) 1:24 porous array, aspect ratio = 3

(5) 1:24 array aspect ratio = 2

(6) 1:24 array aspect ratio = 4

Figure 7. The Different Array Models Tested

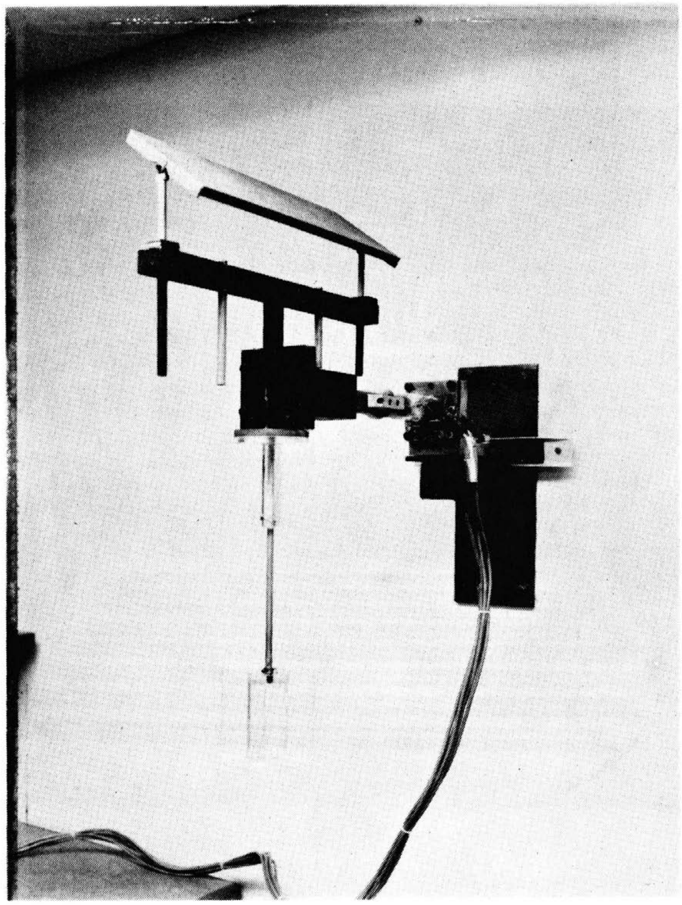

Figure 8. A 1:24 Scale Model Mounted on Force Balance

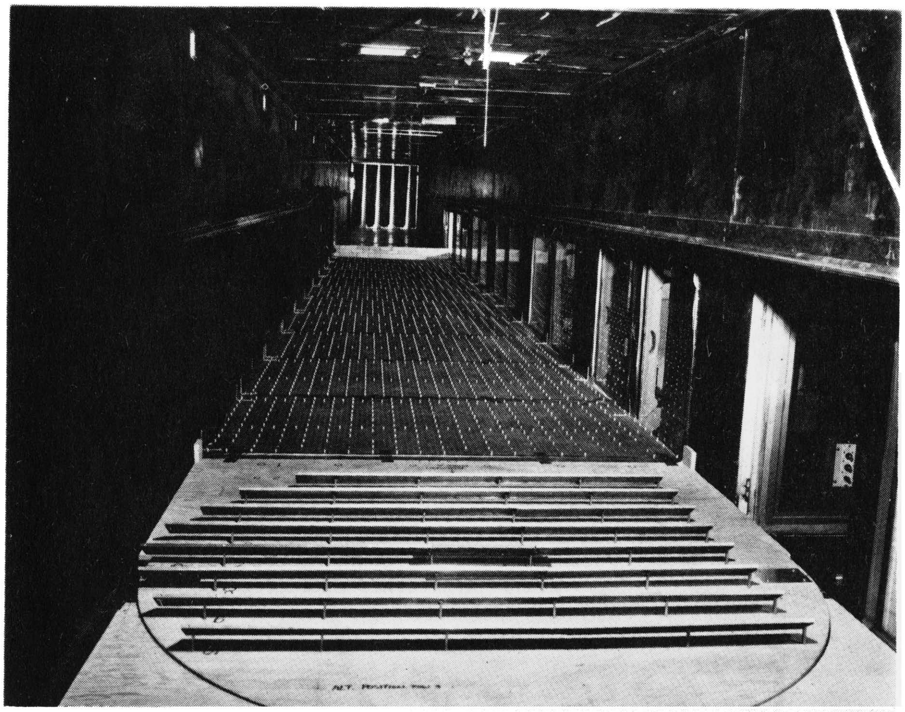

Figure 9. Photograph of Array Field in the Wind Tunnel

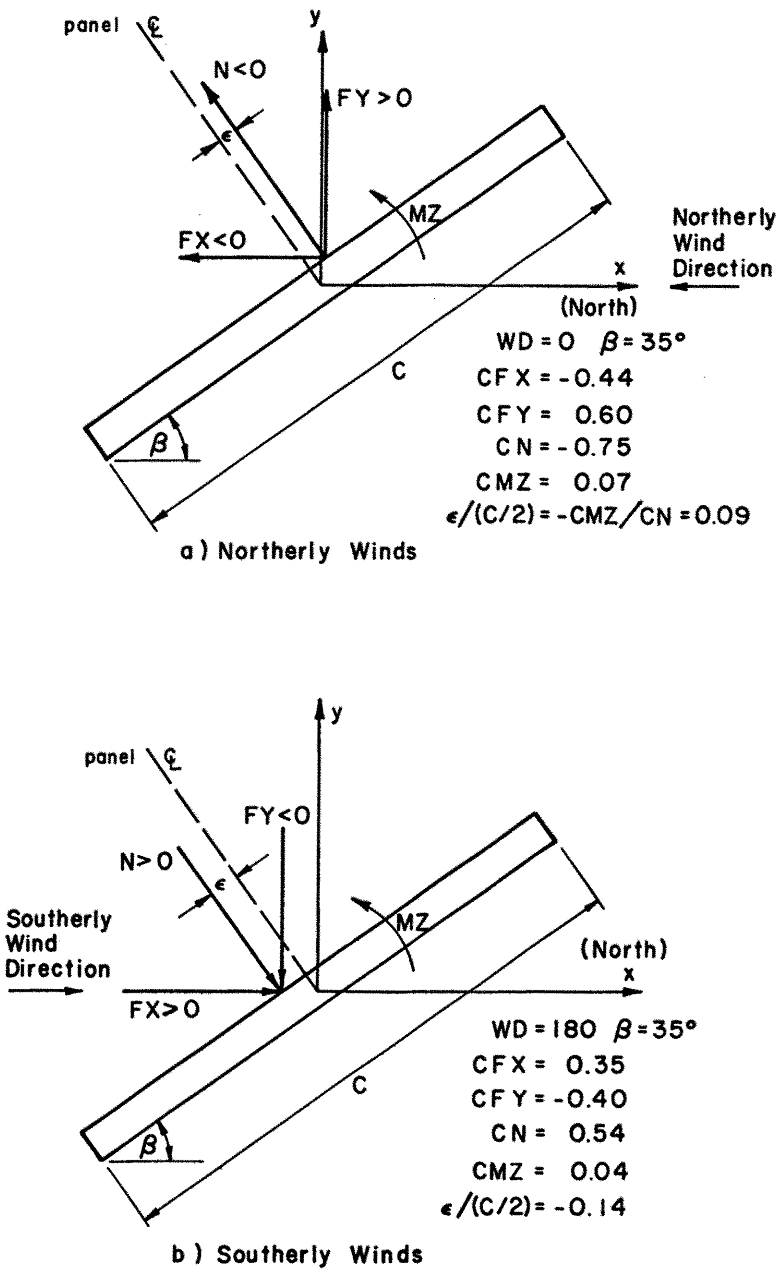

Figure 10. Directions of Forces and Moments for Northerly and Southerly Winds

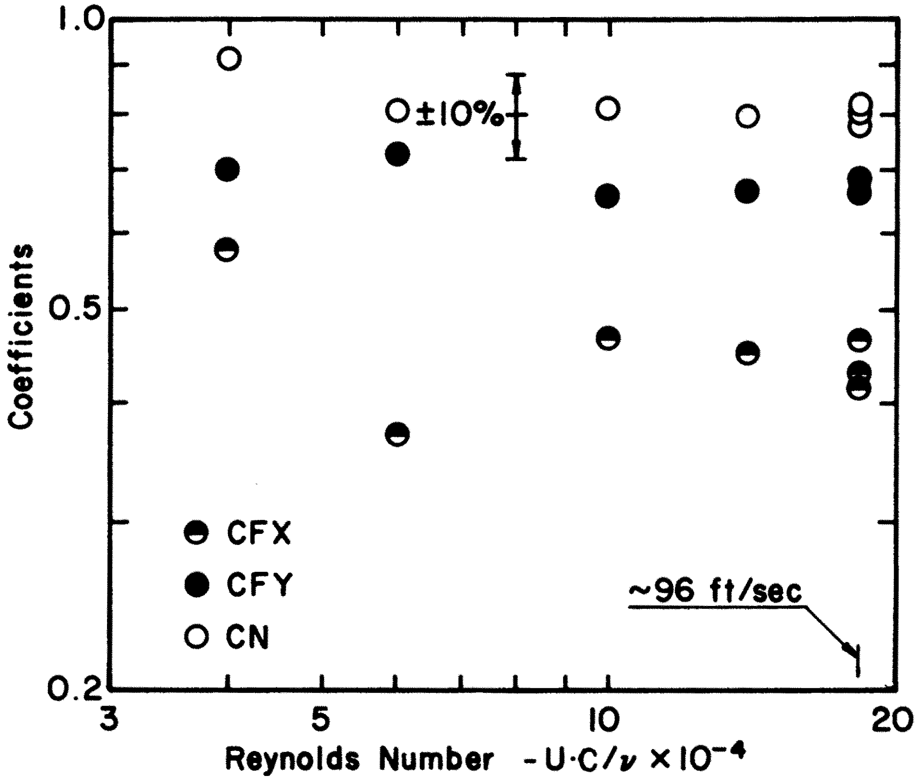

Figure 11. Measurements at Different Reynolds Numbers

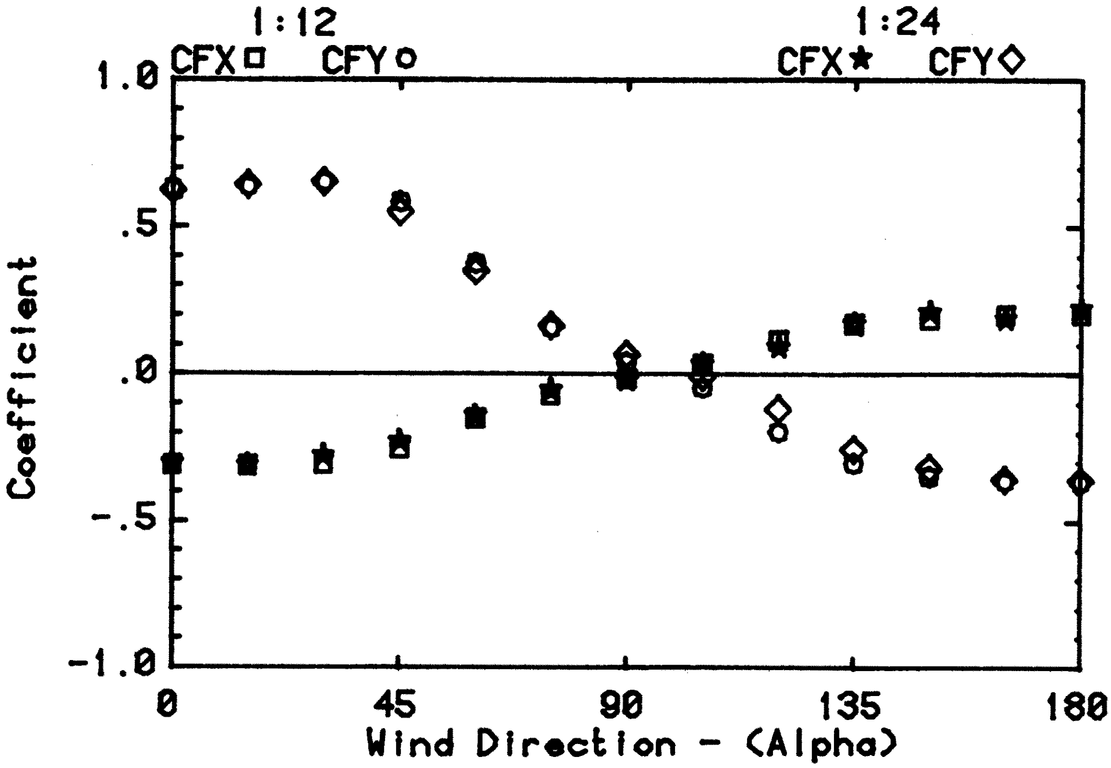

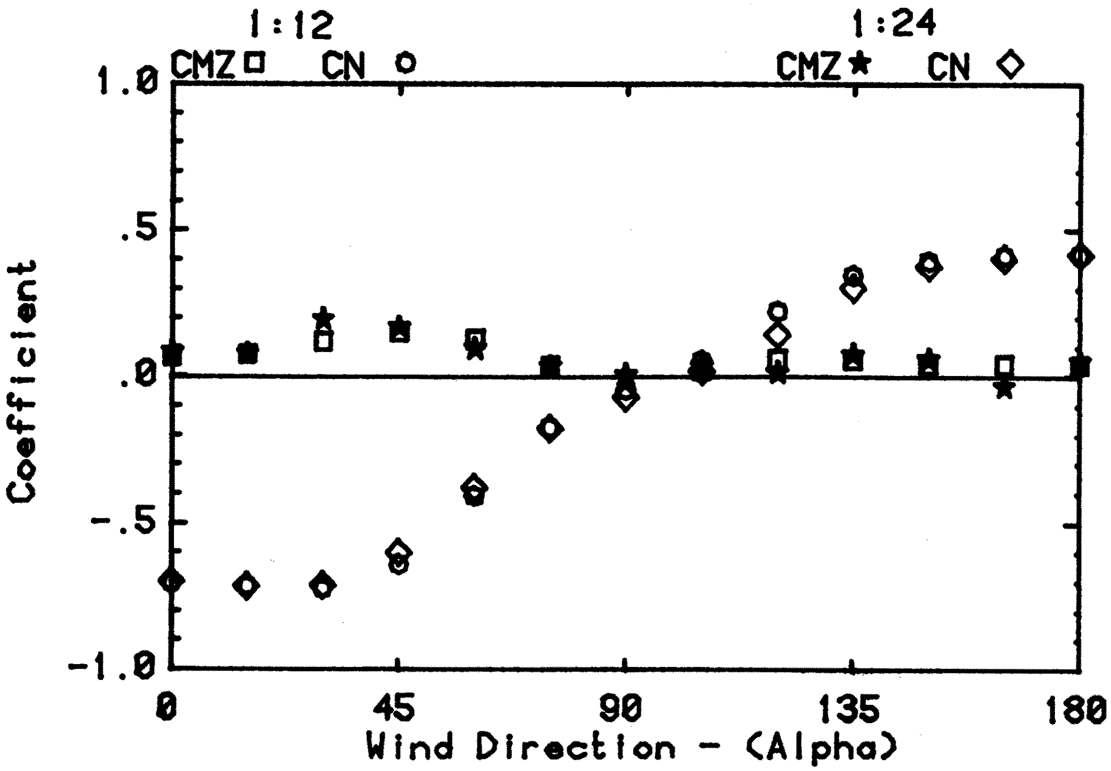

Figure 12. Dimensionless Forces and Moments on a Single Array for $\beta = 25°$, BL1 = 2 ft, Porosity = 0

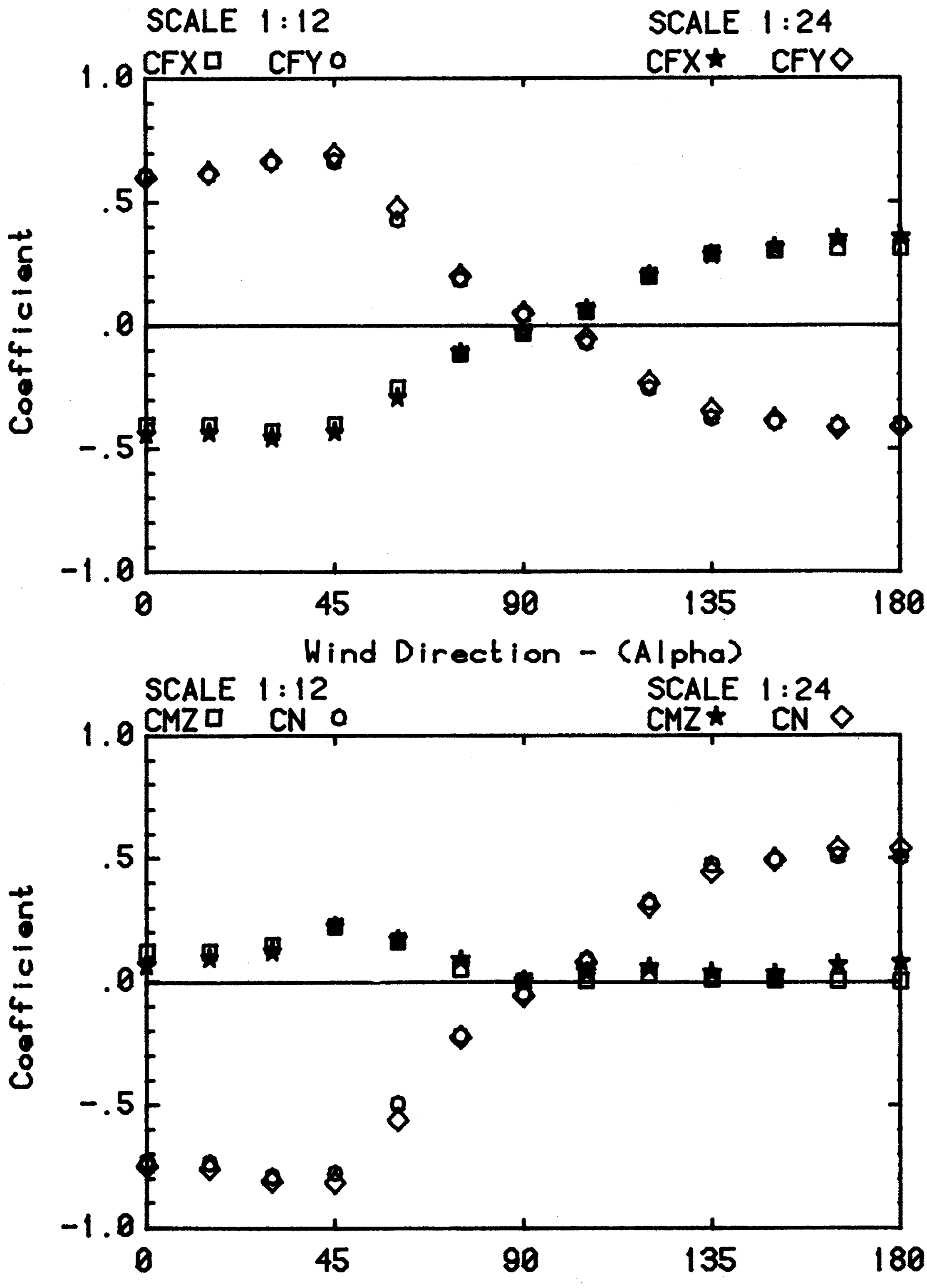

Figure 13. Dimensionless Forces and Moments on a Single Array for $\beta = 35°$, BL1, H = 2 ft, Porosity = 0

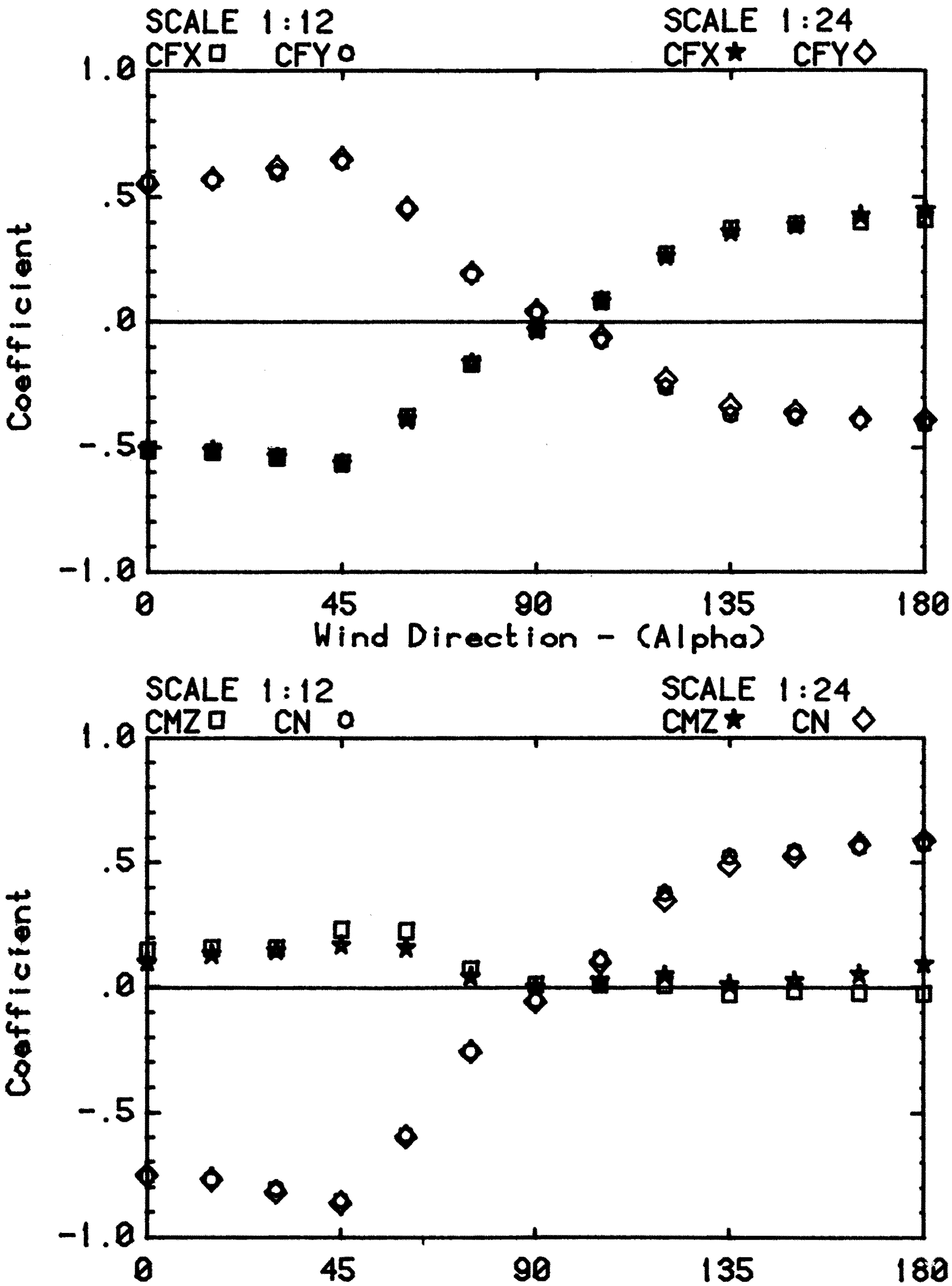

Figure 14. Dimensionless Forces and Moments on a Single Array for $\beta = 45°$, BL1, H = 2 ft, Porosity = 0

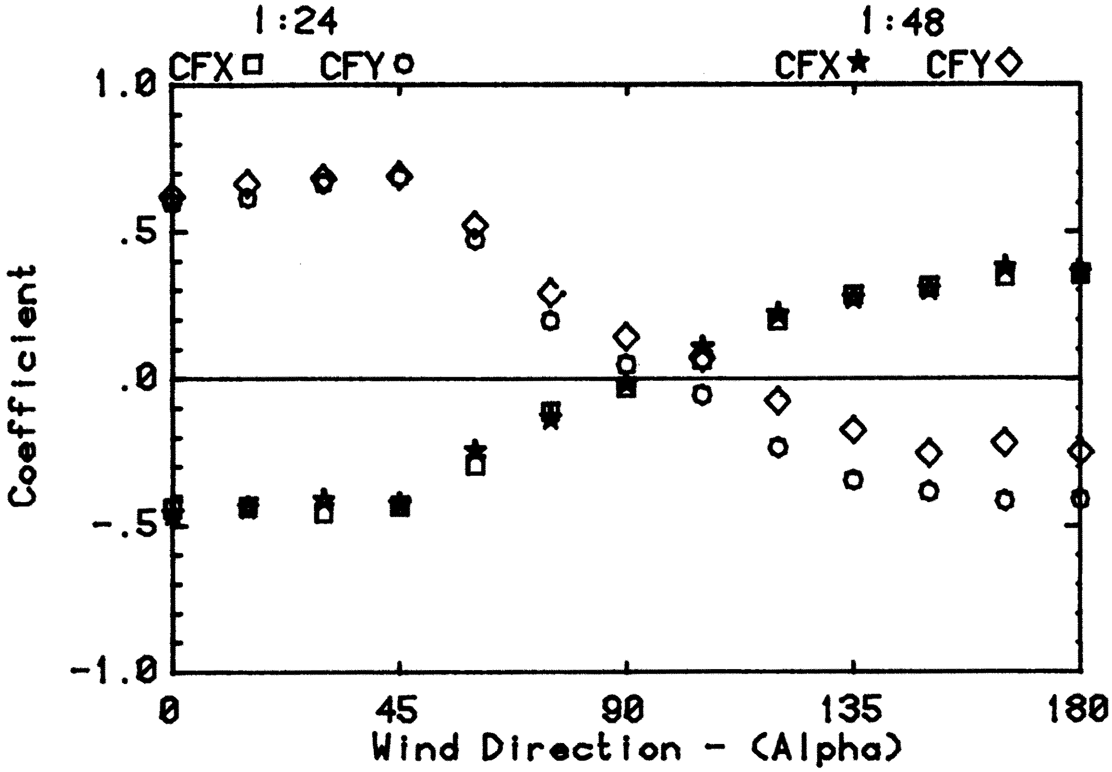

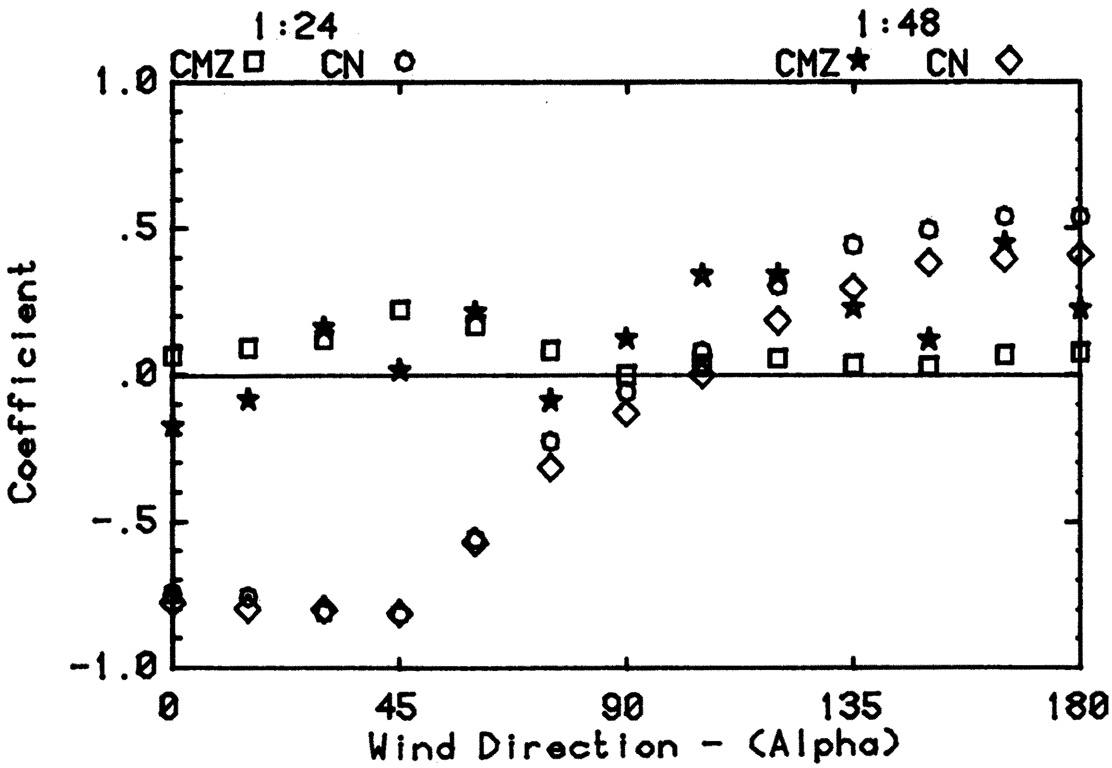

Figure 15. Comparison of the Measurements with the 1:25 and the 1:48 Scale Models for β = 35°, BL1, H = 2 ft, P = 0

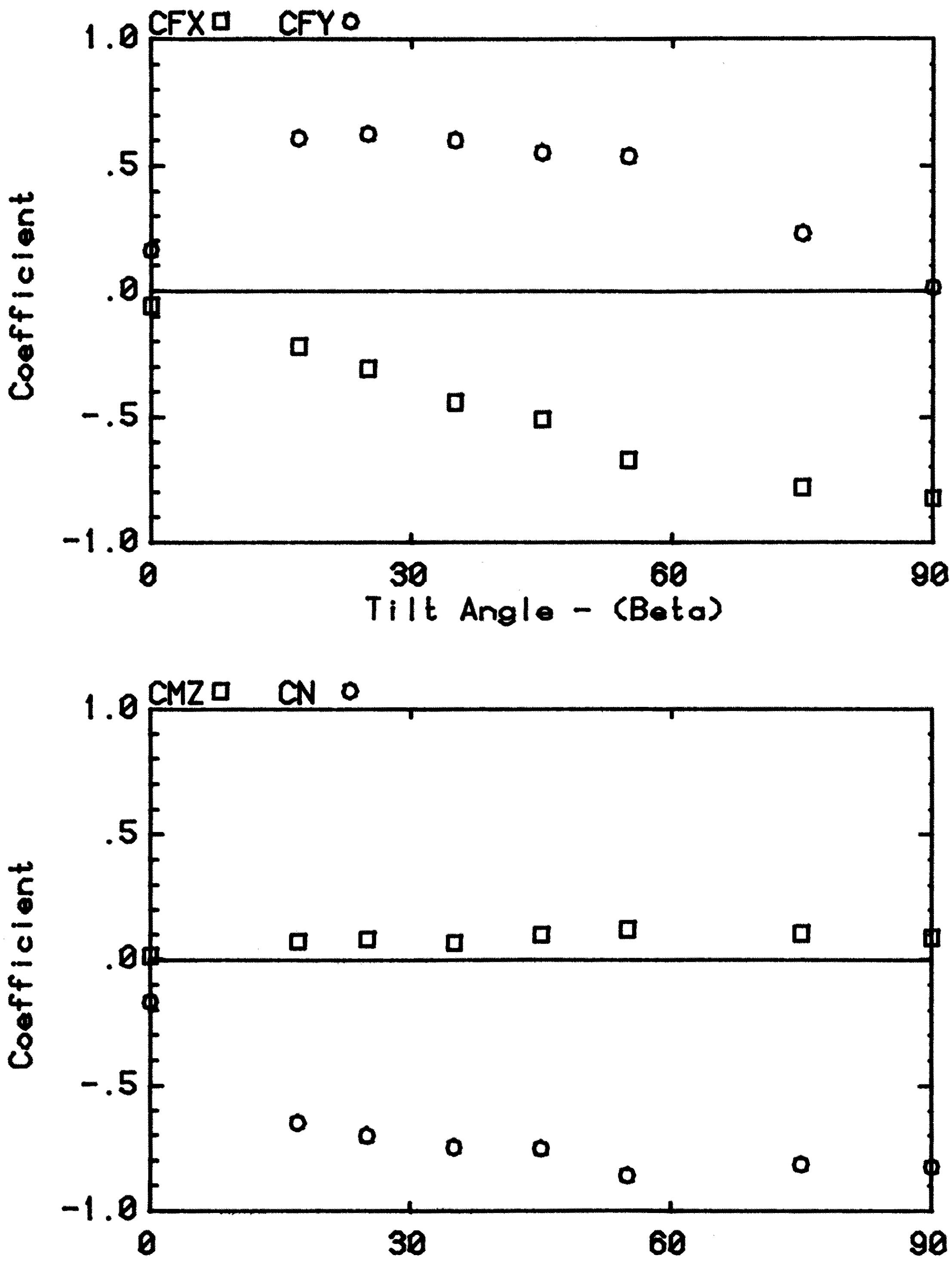

Figure 16. The Dependence of the Aerodynamic Coefficients on β for $\alpha = 0°$, BL1, H = 2 ft, P = 0

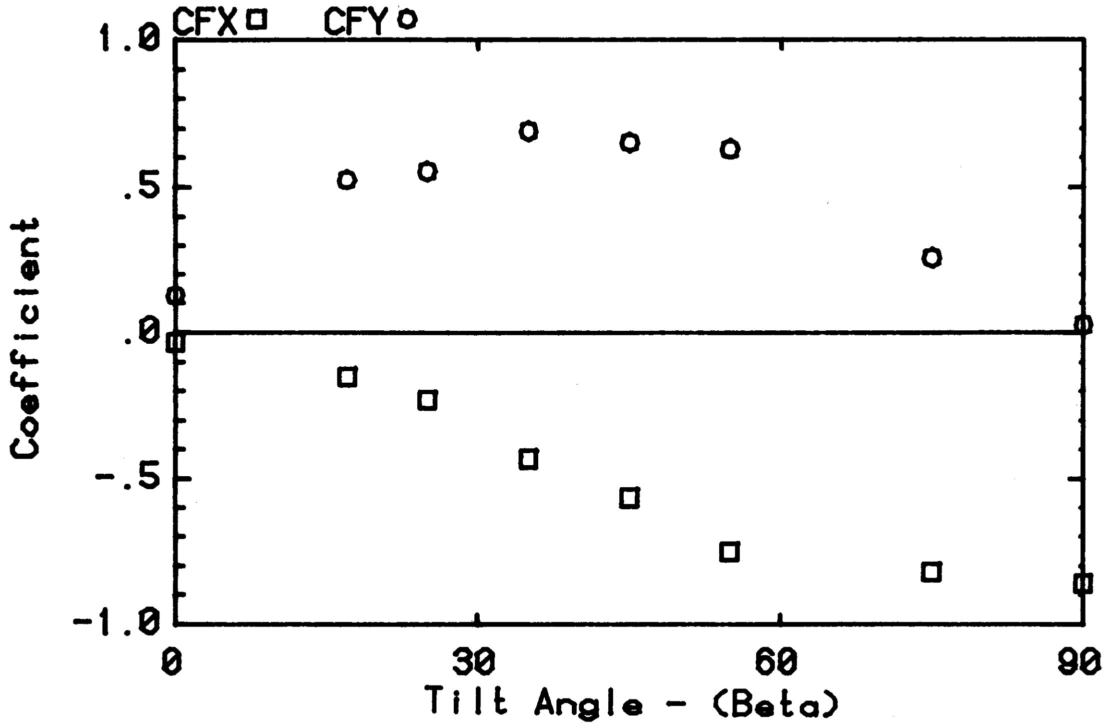

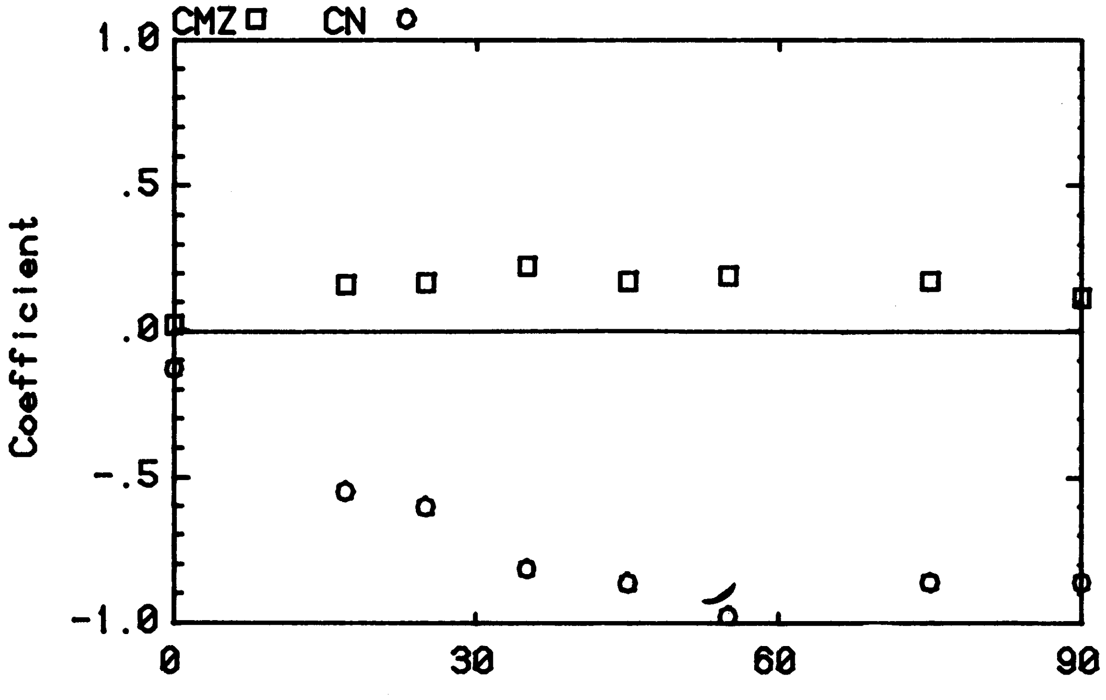

Figure 17. The Dependence of the Aerodynamic Coefficients on β for $\alpha = 45°$, BL1, H = 2 ft, P = 0

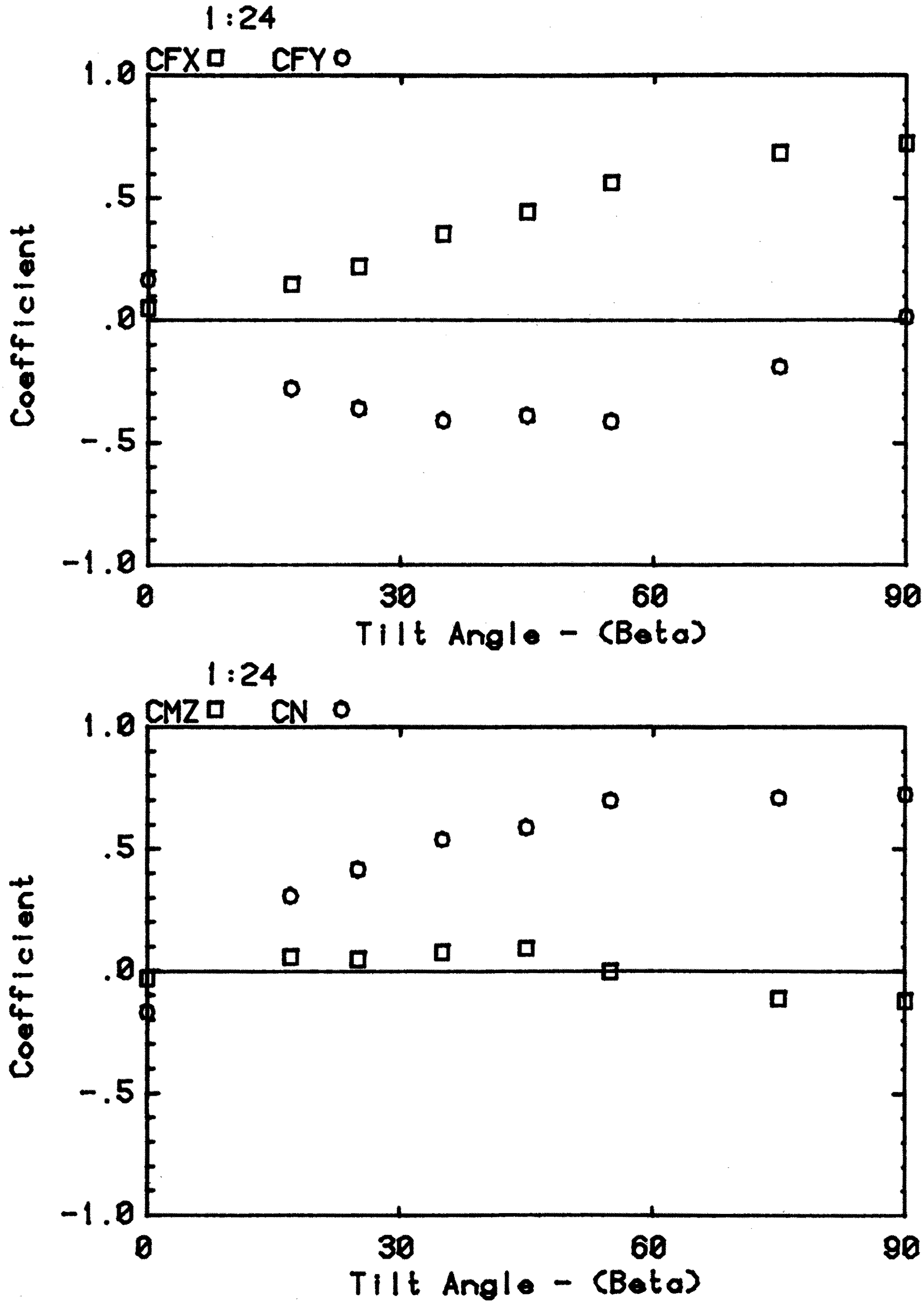

Figure 18. The Dependence of the Aerodynamic Coefficients on β for $\alpha = 180°$, BL1, H = 2 ft, P = 0

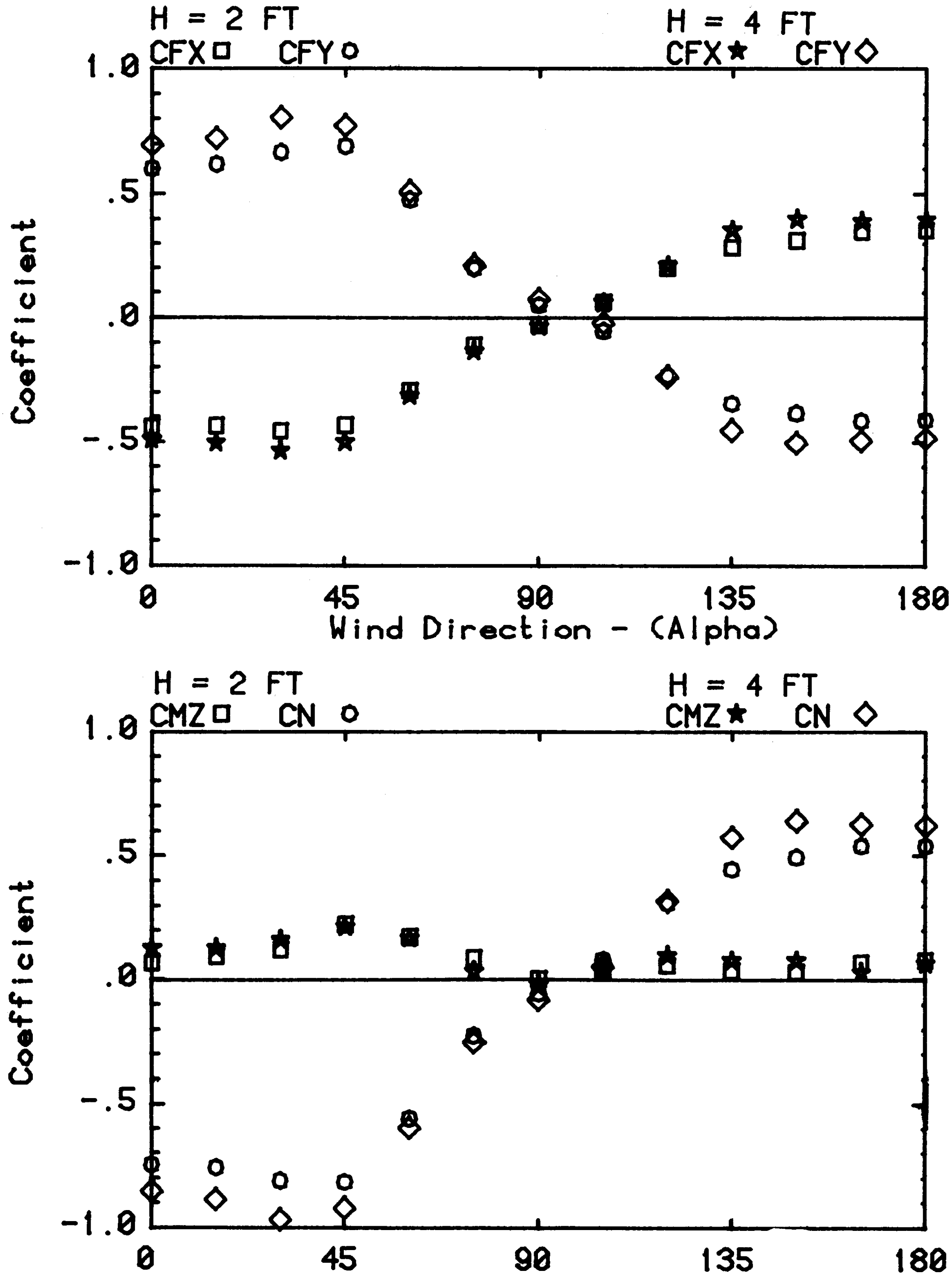

Figure 19. Effect of the Array Height above the Ground, (H = 2 ft and H = 4 ft) for BL1, β = 35°, P = 0

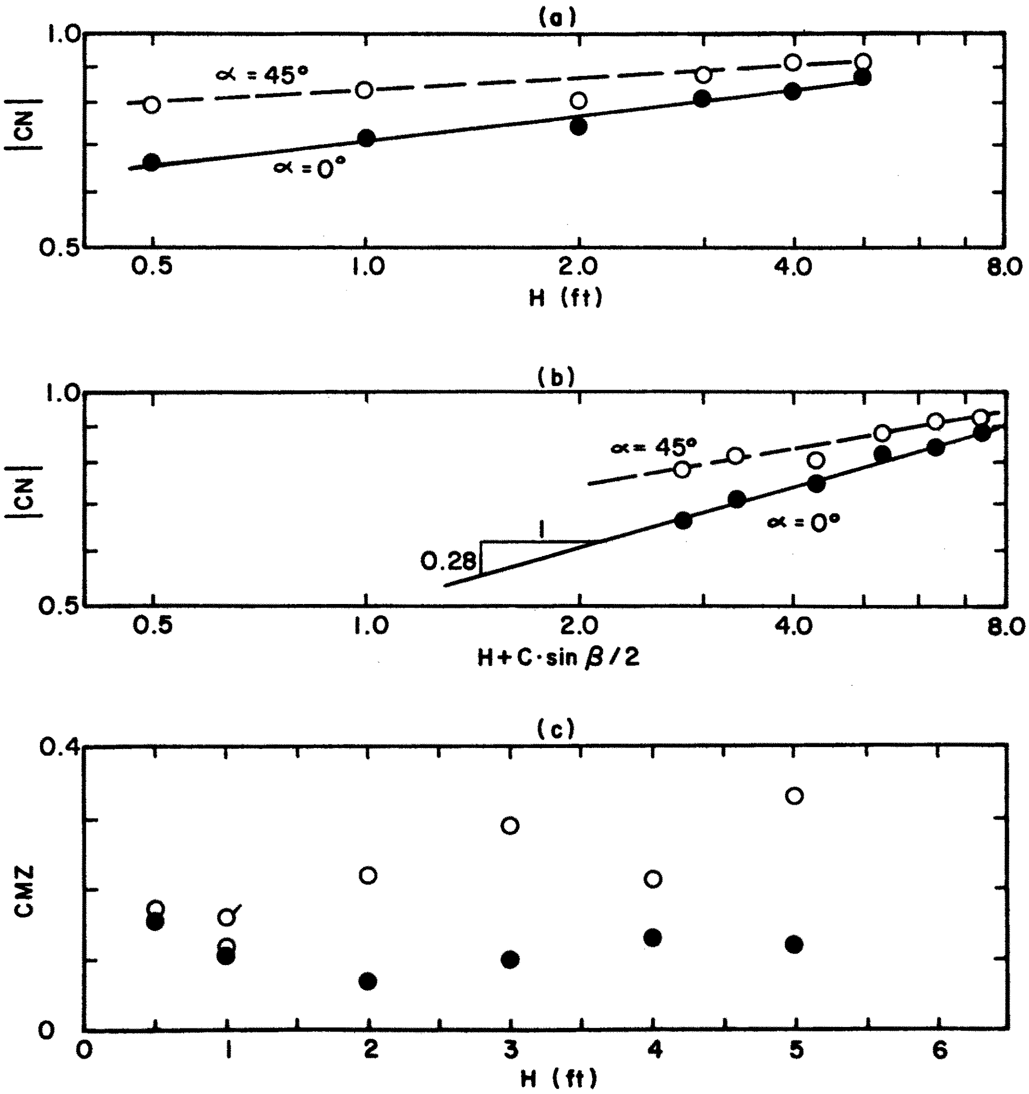

Figure 20. The Effect of the Array Height on CN and CMZ at $\alpha = 0°$, $\alpha = 45°$, $\beta = 35°$

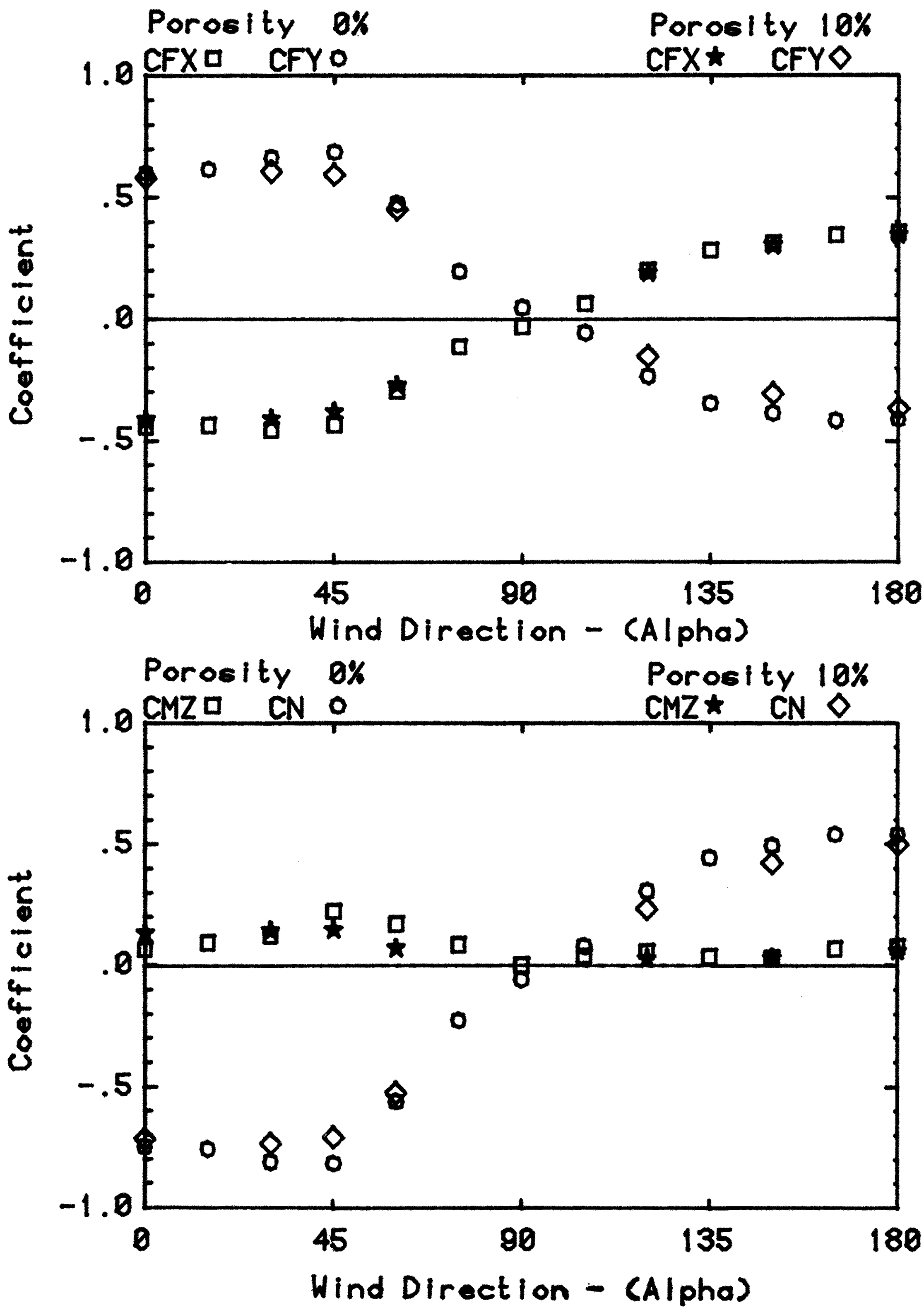

Figure 21. The Effect of the Array Porosity P

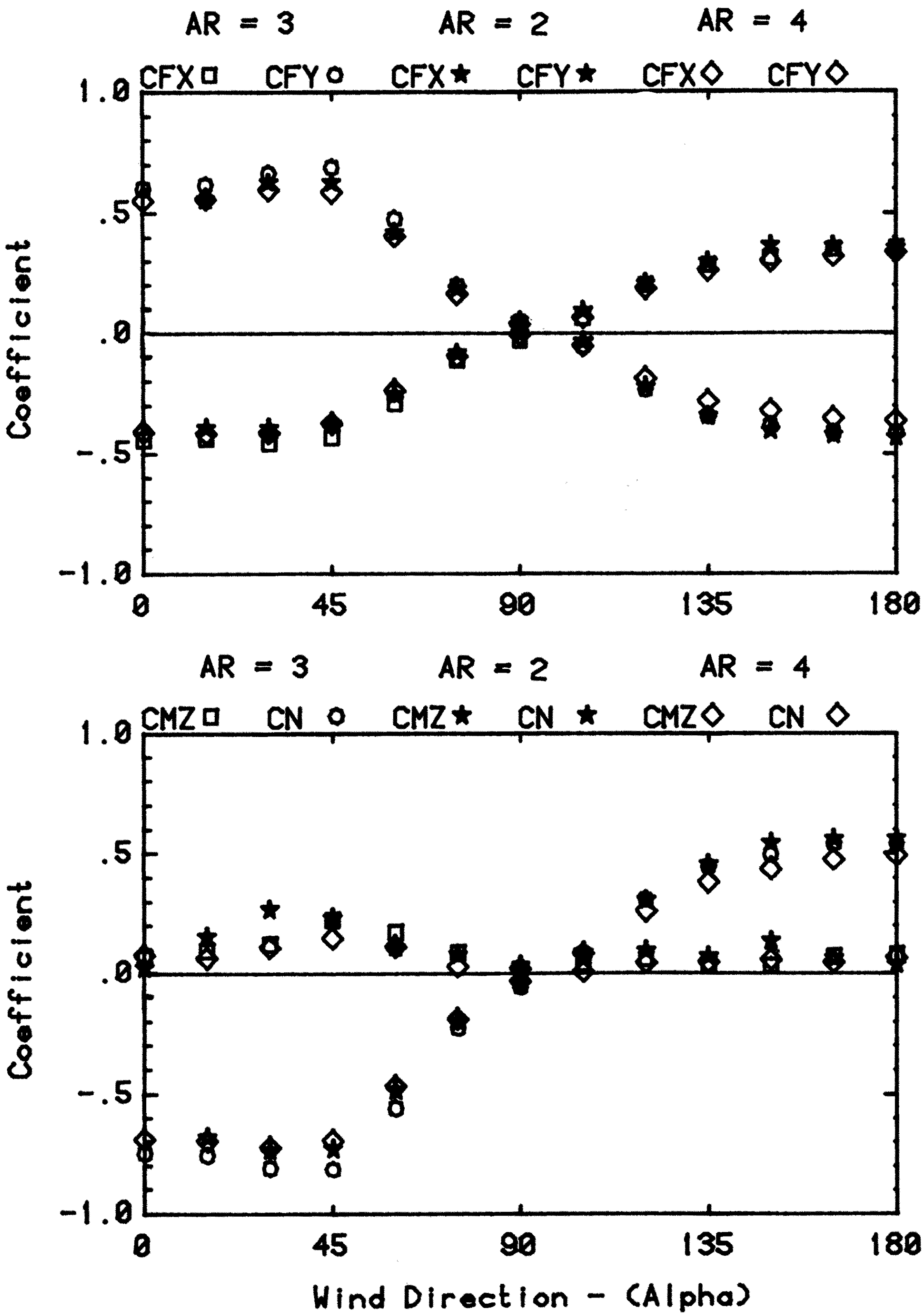

Figure 22. Comparison of Arrays with Different Aspect Ratios for BL1, β = 35°, H = 2 ft, P = 0

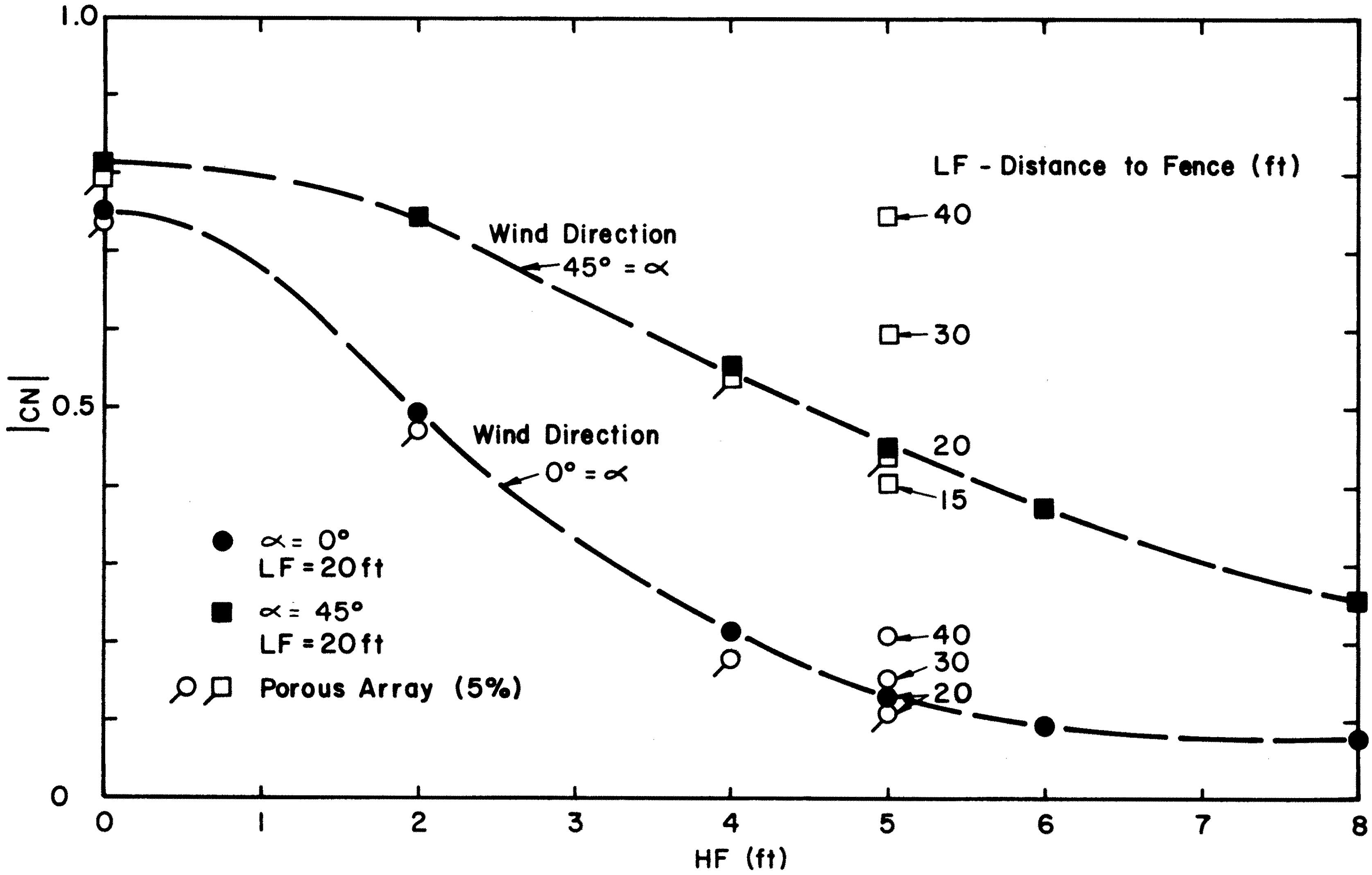

Figure 23. The Effect of a Porous Fence (PF = 30%) on the Normal Force for a Standard Array

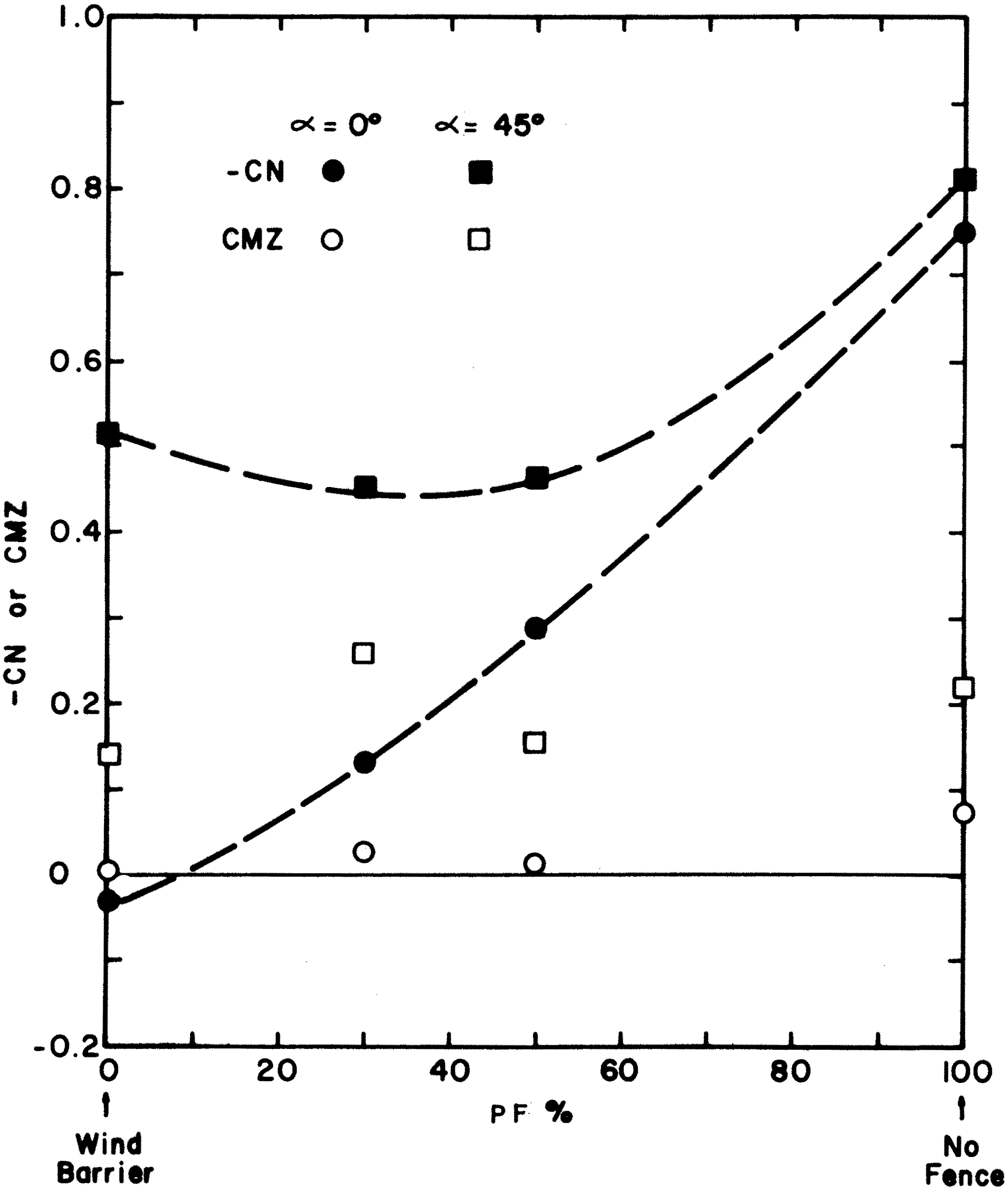

Figure 24. The Effect of the Fence Porosity on a Single Array (LF = 20 ft, FH = 5 ft, H = 2 ft)

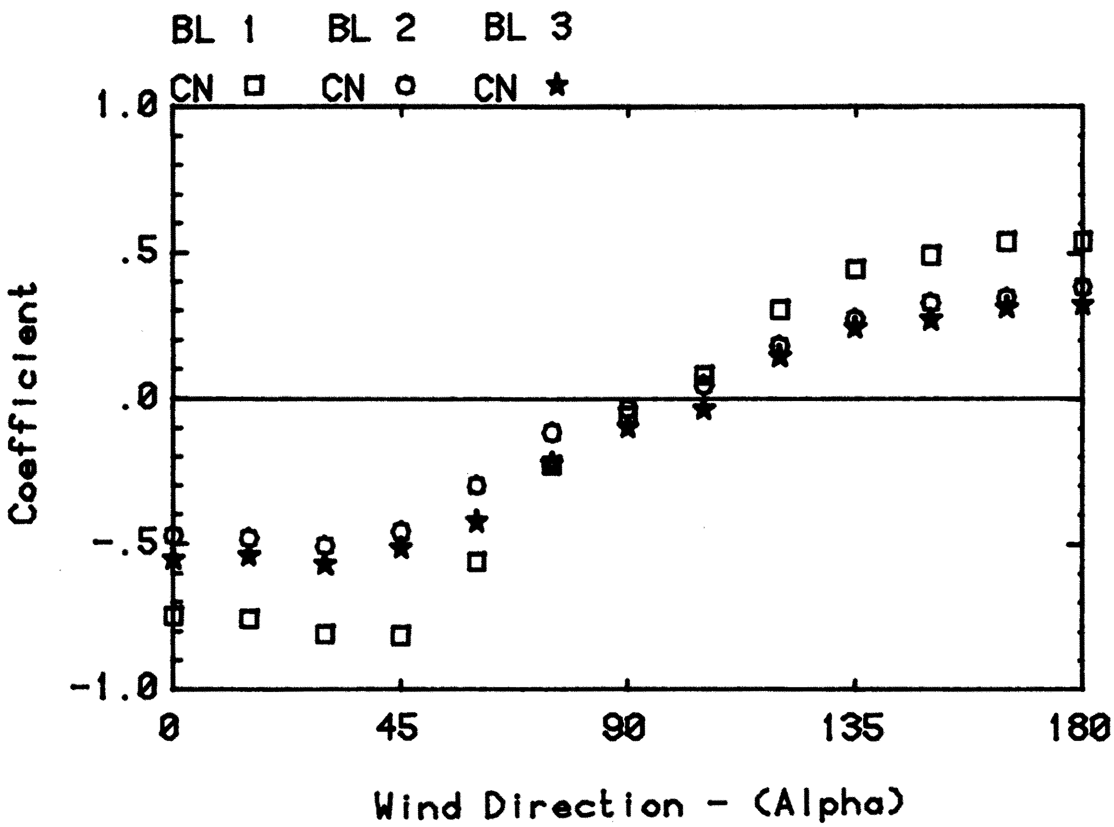

Figure 25. Comparison of the Normal·Force Coefficient in Different Boundary Layers on a Single Array

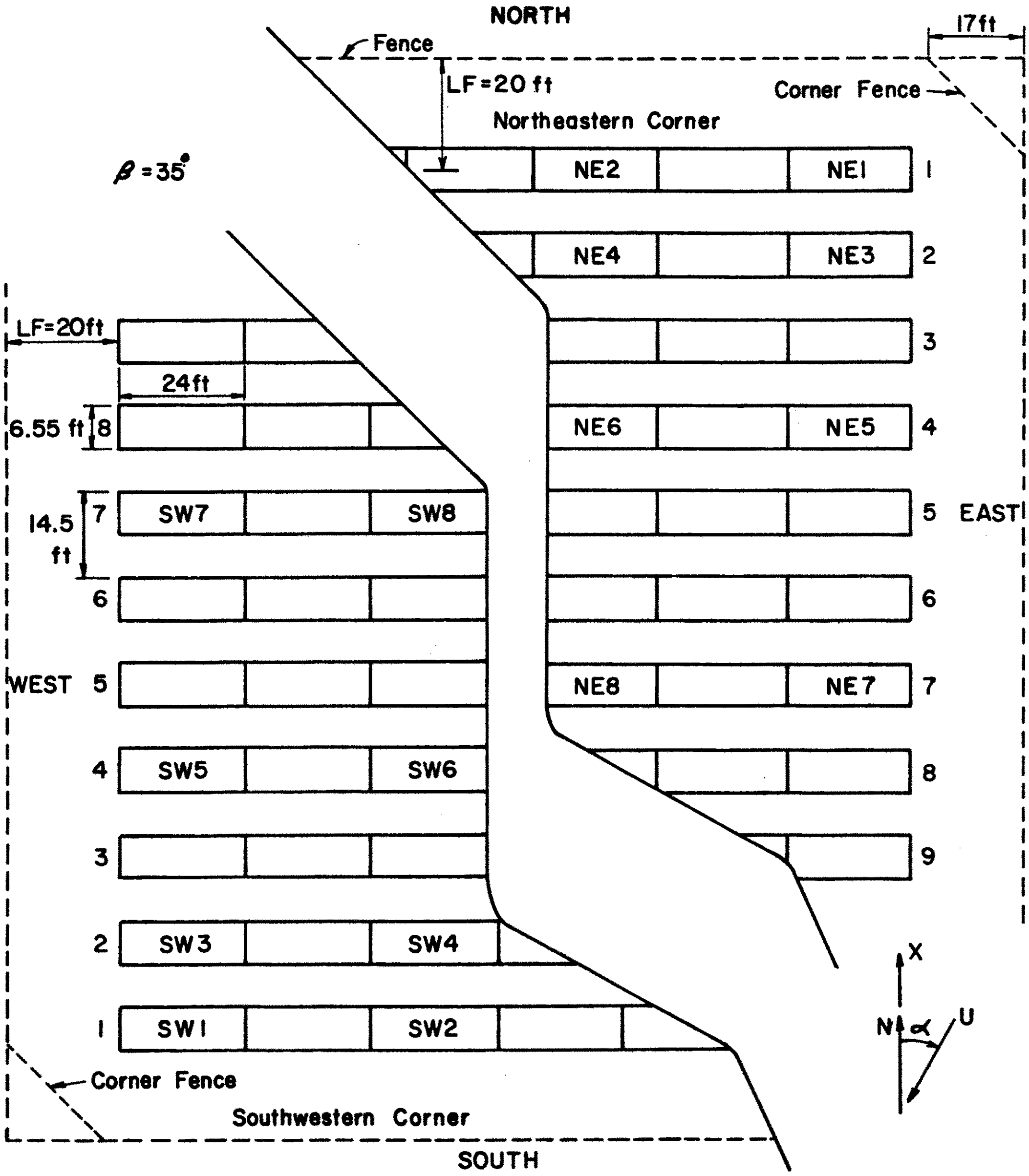

Figure 26. A Schematic Description of the Array Field and the Notation of the Arrays Tested

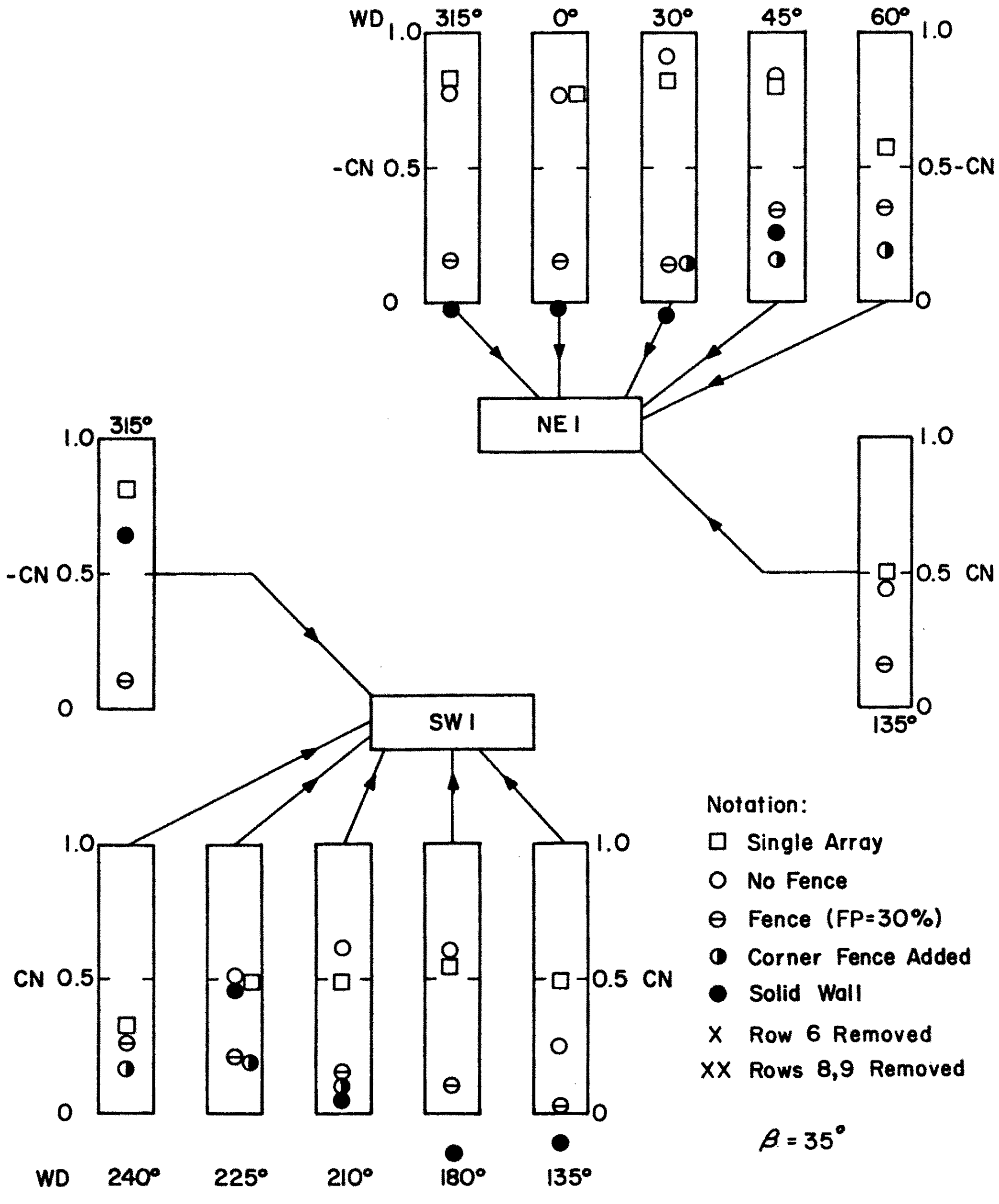

Figure 27. The Normal Force Coefficients for Arrays NE1 and SW1

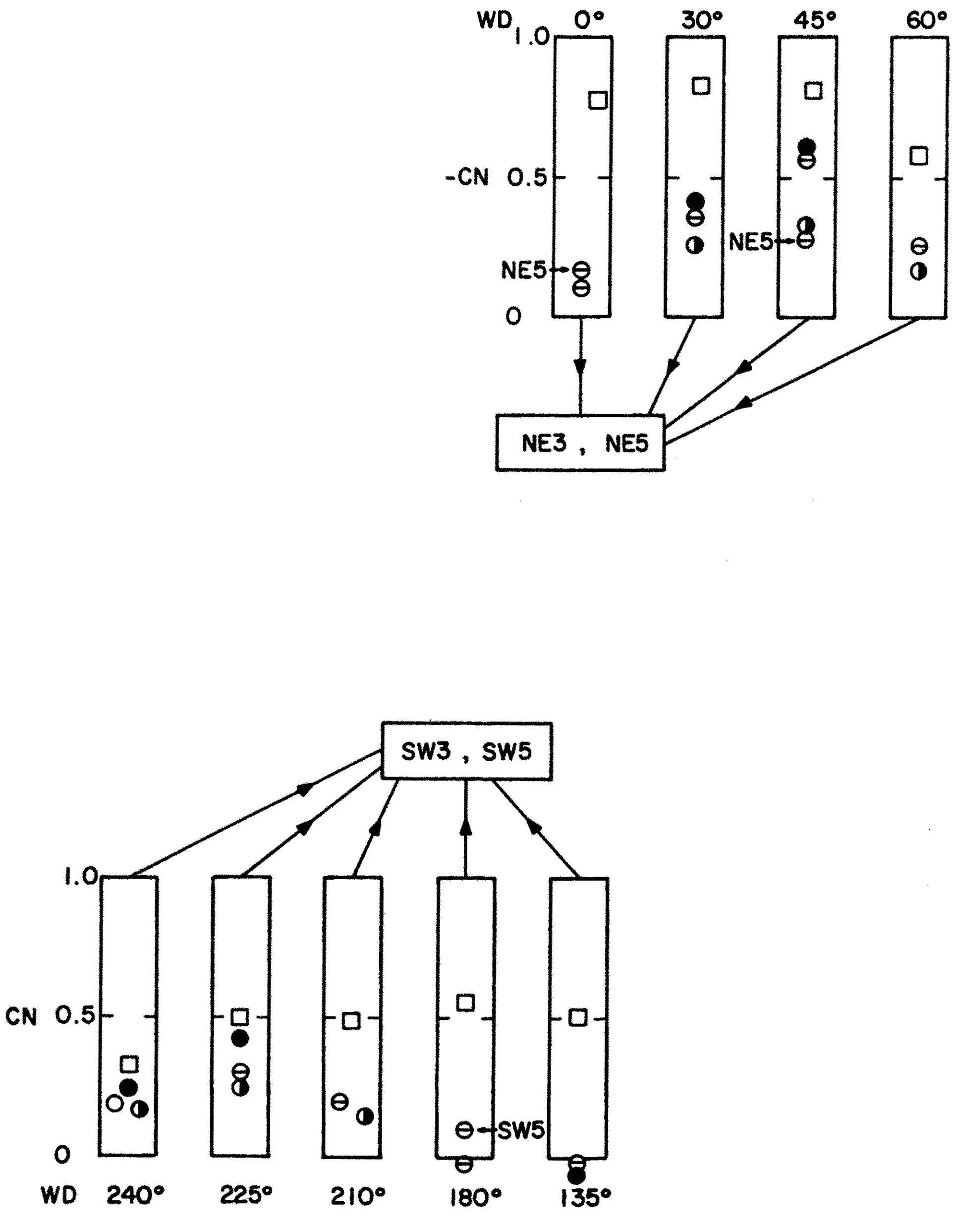

Figure 28. The Normal Force Coefficients for Arrays NE3, SW3, NE5, and SW5

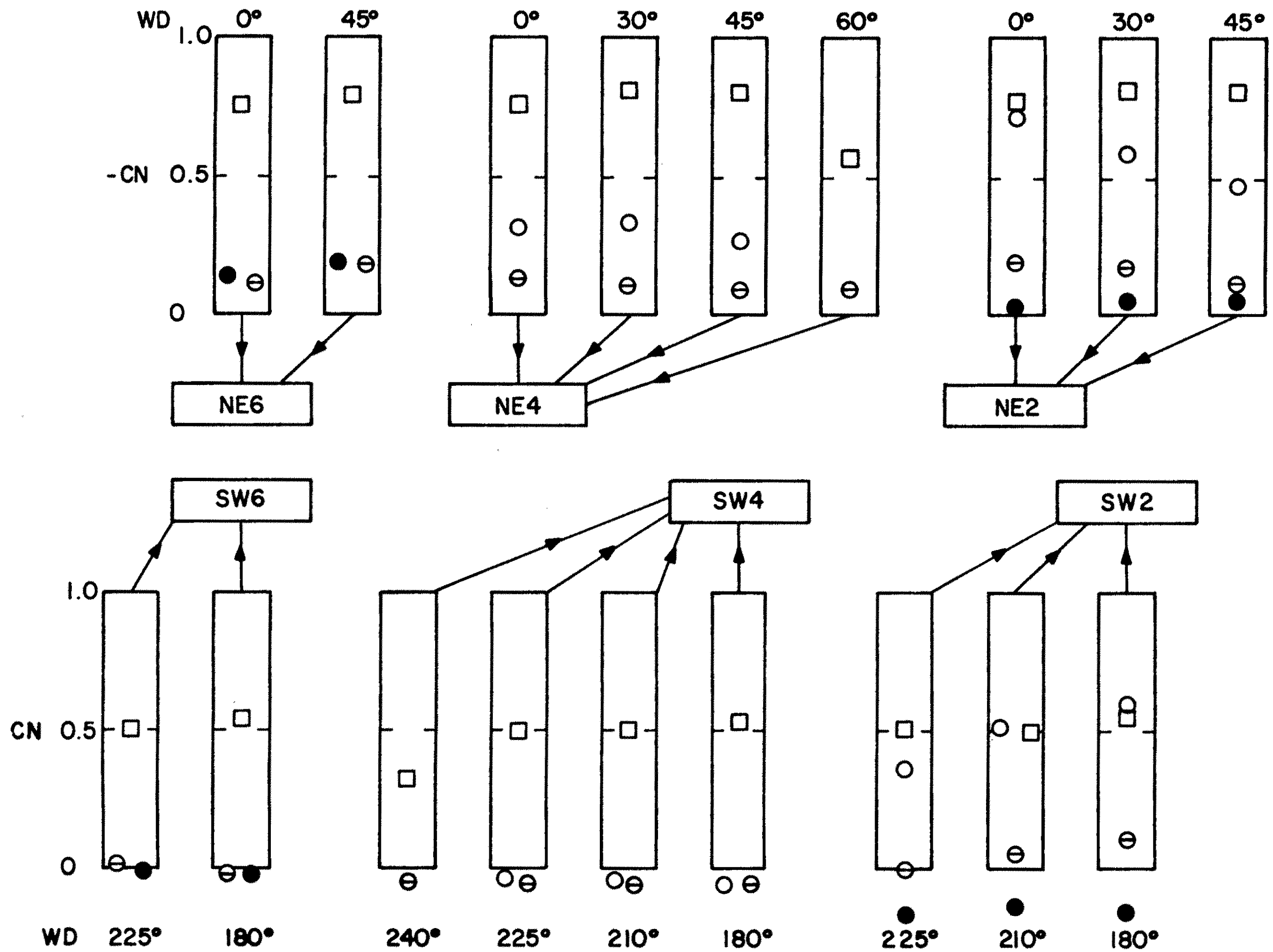

Figure 29. The Normal Force Coefficients for Arrays NE2, NE4, NE6, SW2, SW4, and SW6

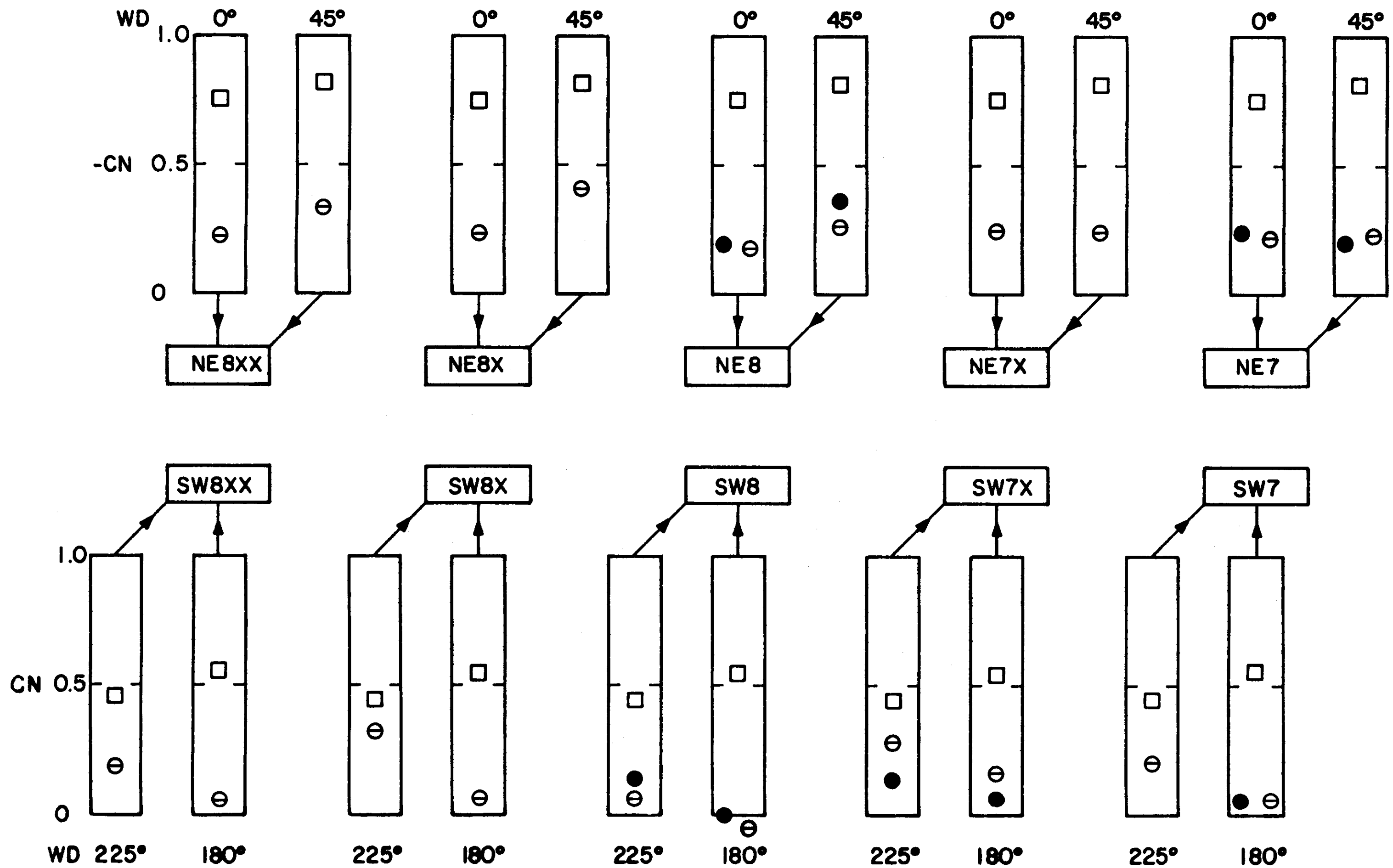

Figure 30. The Normal Force Coefficients for Arrays NE7, SW5, NE8, and SW8

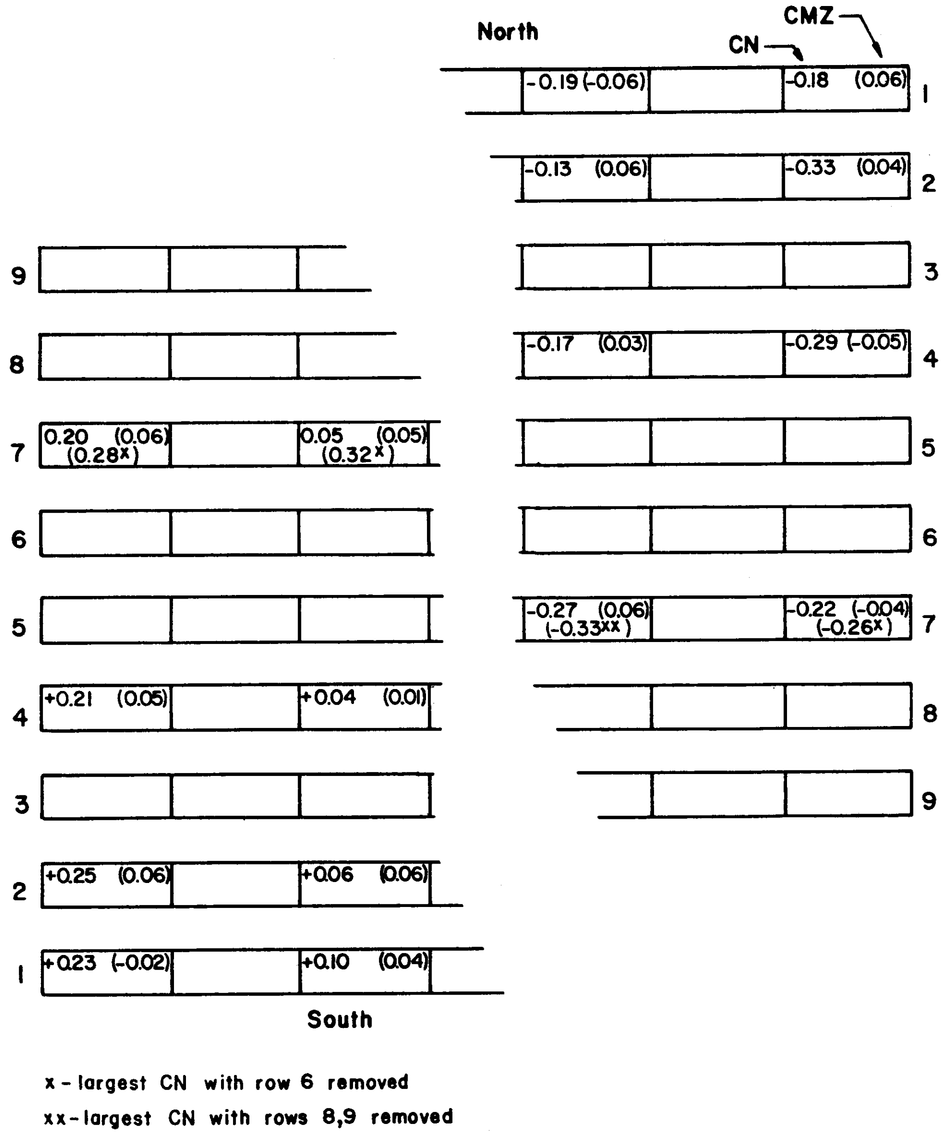

Figure 31. The Maximum Values of the Normal Force and Moment Coefficients in the Array Fields

TABLES

Table 1. Velocity and Turbulence Intensity Profile for Boundary Layer 1

NORMALIZED PROFILE - MTBYL1

PITOT TUBE REFERENCE VELOCITY = 92.34 FT/S

HREF = 50.00 IN

EXPONENT = .1339 U(HMAX) = 90.48

HEIGHT NORMALIZED BY HREF
VELOCITY NORMALIZED BY UREF

DATA POINT	HEIGHT RATIO	UMEAN RATIO	U-RMS RATIO	TURB INT PERCENT
1	.00	.49	.095	19.46
2	.01	.53	.098	18.63
3	.02	.59	.107	18.13
4	.04	.63	.101	15.93
5	.06	.68	.097	14.24
6	.08	.70	.087	12.49
7	.10	.73	.090	12.27
8	.14	.74	.088	11.87
9	.20	.78	.089	11.43
10	.24	.79	.085	10.80
11	.30	.82	.083	10.19
12	.40	.85	.083	9.76
13	.50	.89	.085	9.63
14	.60	.91	.082	9.03
15	.70	.95	.071	7.53
16	.80	.98	.064	6.58
17	1.00	1.00	.046	4.64

Table 2. Velocity and Turbulence Intensity Profile for Boundary Layer 2

NORMALIZED PROFILE - MTBYL2

PITOT TUBE REFERENCE VELOCITY = 93.04 FT/S

HREF = 50.04 IN

EXPONENT = .2373 U(HMAX) = 96.60

HEIGHT NORMALIZED BY HREF
VELOCITY NORMALIZED BY UREF

DATA POINT	HEIGHT RATIO	UMEAN RATIO	U-RMS RATIO	TURB INT PERCENT
1	.00	.32	.090	28.53
2	.01	.34	.103	29.91
3	.02	.40	.116	28.90
4	.04	.46	.125	27.12
5	.06	.53	.120	22.58
6	.08	.56	.122	21.63
7	.10	.61	.125	20.64
8	.14	.66	.117	17.78
9	.20	.71	.107	15.11
10	.24	.75	.105	14.02
11	.32	.79	.096	12.10
12	.40	.85	.096	11.28
13	.50	.90	.084	9.32
14	.60	.93	.075	8.08
15	.70	.96	.064	6.61
16	.80	.99	.054	5.42
17	1.00	1.00	.044	4.37

Table 3. Velocity and Turbulence Intensity Profile for Boundary Layer 3

NORMALIZED PROFILE - MTTURB

PITOT TUBE REFERENCE VELOCITY = 86.20 FT/S

HREF = 49.98 IN

EXPONENT = .1935 U(HMAX) = 79.22

HEIGHT NORMALIZED BY HREF
VELOCITY NORMALIZED BY UREF

DATA POINT	HEIGHT RATIO	UMEAN RATIO	U-RMS RATIO	TURB INT PERCENT
1	.01	.35	.116	33.11
2	.01	.41	.116	28.02
3	.02	.42	.121	28.58
4	.04	.47	.125	26.25
5	.06	.52	.146	27.93
6	.08	.55	.137	24.95
7	.10	.56	.148	26.42
8	.14	.60	.143	23.84
9	.20	.65	.151	23.43
10	.24	.64	.147	23.05
11	.30	.66	.167	25.21
12	.40	.76	.169	22.40
13	.50	.81	.162	19.99
14	.60	.85	.166	19.58
15	.70	.93	.154	16.53
16	.80	.96	.148	15.41
17	1.00	1.00	.144	14.38

Table 4. Test Matrix for Single Array Tests

Scale	BL	H ft	AR	P %	Fence FP %	Fence LF ft	Fence HF ft	β	Wind Azimuth, Degrees 0	15	30	45	60	75	90	105	120	135	150	165	180
1:24	1	2	3	0	-	-	-	0	X			X									X
								17	X			X									X
								25	X	X	X	X	X	X	X	X	X	X	X	X	X
								35	X	X	X	X	X	X	X	X	X	X	X	X	X
								45	X	X	X	X	X	X	X	X	X	X	X	X	X
								55	X			X						X			X
								75	X			X									X
								90	X			X									X
1:48								35	X	X	X	X	X	X	X	X	X	X	X	X	X
1:12								25	X	X	X	X	X	X	X	X	X	X	X	X	X
								35	X	X	X	X	X	X	X	X	X	X	X	X	X
								45	X	X	X	X	X	X	X	X	X	X	X	X	X
								75	X	X	X	X	X	X	X	X	X	X	X	X	X
1:24	2							25	X									X			X
								35	X	X	X	X	X	X	X	X	X	X	X	X	X
								45	X												X
	3							25	X												X
								35	X	X	X	X	X	X	X	X	X	X	X	X	X
								45	X												X
	1	0.5						35	X			X									
		1							X	X	X	X	X	X	X	X	X	X	X	X	X
		3							X			X									
		4							X	X	X	X	X	X	X	X	X	X	X	X	X
		5							X			X									
		2	2							X	X	X	X	X	X	X	X	X	X	X	X
			4						X	X	X	X	X	X	X	X	X	X	X	X	X
			3	2.5					X		X	X	X				X		X		X
				5					X		X	X	X				X		X		X
				10					X		X	X	X				X		X		X
				0	30	15	5					X									
						20			X			X									
						30			X			X									
						40			X			X									
						20	2		X			X									
							4		X			X									
							6		X			X									
							8		X			X									
					0		5		X			X									
					50				X			X									
				5	30				X			X									
							4		X			X									
							2		X			X									

BL = boundary layer
H = height above ground
AR = aspect ratio
P = array porosity
FP = fence porosity
LF = distance to fence
HF = height of fence
β = tilt angle

Table 5. Test Matrix for Array Field Tests

Array No.	Fence in/out	Fence Porosity %	Wind Azimuth, degrees 0	30	45	60	135	180	210	225	240	315
NE1	in	30	X	X	X	X	X					
	in	0	X	X	X							
	out	-	X	X	X							X
	in*	30		X	X	X						
SW1	in	30					X	X	X	X	X	X
	in	0					X	X	X	X		
	out	-					X	X	X	X		X
	in*	30							X	X	X	
NE2	in	30	X	X	X							
	in	0	X	X	X							
	out	-	X	X	X							
SW2	in	30						X	X	X		
	in	0						X	X	X		
	out	-						X	X	X		
NE3	in	30	X	X	X	X						
	in	0		X	X							
	in*	30		X	X	X						
SW3	in	30					X	X	X	X	X	
	in	0					X			X	X	
	in*	30							X	X	X	
NE4	in	30	X	X	X	X						
	out	-	X	X	X							
SW4	in	30						X	X	X	X	
	out	-						X	X	X		
NE5	in	30	X		X							
SW5	in	30						X		X		
NE6	in	30	X		X							
	in	0	X		X							
SW6	in	30						X		X		
	in	0						X		X		
NE7	in	30	X		X							
	in	0	X		X							
NE7X	in	30	X		X							
SW7	in	30						X		X		
	in	0						X		X		
SW7X	in	30						X		X		
NE8	in	30	X		X							
	in	0	X		X							
NE8X	in	30	X		X							
NE8XX	in	30	X		X							
SW8	in	30						X		X		
	in	0						X		X		
SW8X	in	30						X		X		
SW8XX	in	30						X		X		

Array Number - See Fig. 26 for numbering system
X in array number indicates row 6 arrays removed
XX in array number indicates rows 8, 9 removed

Fence Configuration - in = perimeter fence in place (see Fig. 26)
in* = corner diagonal included (see Fig. 26)
out = fence removed

APPENDIX A

AERODYNAMIC COEFFICIENTS FOR A SINGLE ARRAY AND AN ARRAY FIELD

DATA FILE NAME CODE

1. Single Array Study

File name has structure: $\underset{1}{\underline{S}}\ \underset{2}{\underline{1}}\ \underset{3}{\underline{24}}\ \underset{4}{\underline{2}}\ \underset{5}{\underline{0}}$ (Element)

Element 1 is array configuration:

S = single standard array

A = array with aspect ratio 2 (8 ft x 16 ft)

B = array with aspect ratio 4 (8 ft x 32 ft)

D = standard array plus porosity

F = standard array with fence upwind

A. For Element 1 = S, A, B, or D

Element 2 is approach boundary layer:

1 = boundary layer 1 (BL1)

2 = boundary layer 2 (BL2)

3 = boundary layer 3 (BL3)

Element 3 is model scale:

12 = scale 1:12

24 = scale 1:24

48 = scale 1:48

Element 4 is height of array (see Figure 3):

0 : H = 0.5 ft

1 : H = 1.0 ft

2 : H = 2.0 ft

3 : H = 3.0 ft

4 : H = 4.0 ft

5 : H = 5.0 ft

Element 5 is array porosity (P):

0 : P = 0

1 : P = 2.5%

2 : P = 5%

3 : P = 10%

B. For Element 1 = F

Element 2 is fence porosity (FP):

1 : FP = 0% (solid fence)

2 : FP = 30%

3 : FP = 50%

Element 3 is distance from array to fence (LF):

15 : LF = 15 ft

20 : LF = 20 ft

30 : LF = 30 ft

40 : LF = 40 ft

Element 4 is height of fence (HF):

2 : HF = 2 ft

4 : HF = 4 ft

5 : HF = 5 ft

6 : HF = 6 ft

8 : HF = 8 ft

Element 5 is array porosity (P):

0 : P = 0

5 : P = 5%

2. Array Field Study

File name has structure : $\underline{\text{NE 1}}$ $\underline{\text{F30}}$
Element 1 2

Element 1 is unit number in field array (see Fig. 26)

Element 2 is fence configuration or row removal configuration:

000 = no fence

F30 = fence with porosity 30%

F00 = fence with no porosity (solid)

S30 = special corner fence included, FP = 30%

30X = fence porosity 30% with field row 6 removed

3XX = fence porosity 30% with field rows 8, 9 removed

DATA FOR FILE: S12420

SINGLE STANDARD ARRAY - BL1, SCALE 1:24, H = 2 FT, P = 0

RUN #	BETA	WIND	CFX	CFY	CN	CMZ
350	0	0	-.06	.16	-.16	.02
351	0	45	-.03	.13	-.13	.02
349	0	180	.05	.17	-.17	-.03
240	17	0	-.22	.61	-.65	.07
241	17	45	-.15	.53	-.55	.16
242	17	180	.15	-.28	.31	.06
239	25	0	-.31	.63	-.70	.08
238	25	15	-.31	.65	-.72	.08
237	25	30	-.28	.65	-.71	.19
236	25	45	-.23	.55	-.60	.17
235	25	60	-.14	.35	-.38	.10
234	25	75	-.05	.17	-.17	.03
233	25	90	-.02	.07	-.07	.01
232	25	105	.03	-.00	.02	.03
231	25	120	.09	-.12	.14	.01
229	25	135	.17	-.26	.30	.07
228	25	150	.21	-.32	.38	.06
227	25	165	.19	-.36	.40	-.03
226	25	180	.22	-.36	.42	.05
205	35	0	-.44	.60	-.75	.07
204	35	15	-.43	.62	-.76	.10
203	35	30	-.46	.67	-.81	.12
202	35	45	-.43	.69	-.81	.22
201	35	60	-.29	.48	-.56	.17
200	35	75	-.11	.20	-.23	.09
199	35	90	-.03	.05	-.06	.00
198	35	105	.07	-.05	.08	.04
196	35	120	.20	-.23	.31	.06
195	35	135	.28	-.34	.44	.04
194	35	150	.31	-.38	.49	.03
193	35	165	.35	-.42	.54	.07
192	35	180	.35	-.41	.54	.08
218	45	0	-.51	.55	-.75	.10
217	45	15	-.51	.57	-.77	.13
216	45	30	-.54	.62	-.82	.15
215	45	45	-.57	.65	-.86	.17
214	45	60	-.39	.45	-.60	.16
213	45	75	-.16	.20	-.25	.04
212	45	90	-.03	.05	-.06	-.00
211	45	105	.08	-.06	.10	.03
210	45	120	.26	-.23	.35	.05
209	45	135	.36	-.34	.49	.01
208	45	150	.38	-.36	.53	.02
207	45	165	.42	-.39	.57	.05
206	45	180	.45	-.39	.59	.09
223	55	0	-.67	.54	-.86	.12
222	55	45	-.75	.63	-.98	.19
221	55	135	.50	-.36	.61	.02
220	55	180	.57	-.41	.70	-.00
247	75	0	-.78	.23	-.81	.11
246	75	45	-.82	.26	-.86	.17
248	75	180	.69	-.19	.71	-.11
244	90	0	-.82	.02	-.82	.09
245	90	45	-.86	.03	-.86	.11
243	90	180	.72	.02	.72	-.12

DATA FOR FILE: S14820

SINGLE STANDARD ARRAY - BL1, SCALE 1:48, H = 2 FT, P = 0

RUN #	BETA	WIND	CFX	CFY	CN	CMZ
468	35	0	-.46	.62	-.78	-.17
467	35	15	-.44	.67	-.80	-.08
466	35	30	-.41	.69	-.80	.16
465	35	45	-.43	.69	-.81	.02
464	35	60	-.24	.52	-.57	.21
463	35	75	-.13	.29	-.32	-.09
462	35	90	-.02	.15	-.13	.12
461	35	105	.11	.07	.00	.34
460	35	120	.22	-.07	.19	.34
459	35	135	.27	-.17	.30	.23
458	35	150	.30	-.25	.38	.12
457	35	165	.38	-.22	.40	.45
456	35	180	.36	-.25	.41	.23

DATA FOR FILE: S11220

SINGLE STANDARD ARRAY - BL1, SCALE 1:12, H = 2 FT, P = 0

RUN #	BETA	WIND	CFX	CFY	CN	CMZ
292	25	0	-.31	.63	-.70	.07
293	25	15	-.31	.64	-.71	.08
294	25	30	-.31	.66	-.72	.12
295	25	45	-.25	.59	-.64	.15
296	25	60	-.15	.38	-.41	.13
297	25	75	-.07	.16	-.17	.04
298	25	90	-.01	.04	-.04	.22
299	25	105	.03	-.04	.05	.02
300	25	120	.12	-.19	.22	.06
301	25	135	.17	-.30	.35	.06
302	25	150	.19	-.35	.39	.04
303	25	165	.20	-.36	.41	.04
304	25	180	.21	-.36	.42	.04
291	35	0	-.40	.61	-.73	.12
290	35	15	-.40	.61	-.74	.12
289	35	30	-.43	.66	-.79	.15
288	35	45	-.40	.67	-.78	.23
287	35	60	-.25	.43	-.50	.16
286	35	75	-.11	.19	-.22	.05
285	35	90	-.03	.04	-.05	-.00
284	35	105	.06	-.07	.09	.00
283	35	120	.20	-.25	.32	.03
282	35	135	.29	-.37	.47	.01
281	35	150	.30	-.39	.49	.01
280	35	165	.31	-.40	.51	.00
279	35	180	.31	-.40	.51	.00
266	45	0	-.51	.56	-.76	.15
267	45	15	-.52	.57	-.77	.16
268	45	30	-.54	.60	-.80	.16
269	45	45	-.56	.64	-.85	.23
270	45	60	-.38	.45	-.59	.23
271	45	75	-.17	.19	-.25	.08
272	45	90	-.03	.04	-.05	.01
273	45	105	.09	-.07	.11	.01
274	45	120	.27	-.26	.38	.01
275	45	135	.37	-.37	.52	-.03
276	45	150	.39	-.38	.54	-.01
277	45	165	.40	-.39	.56	-.02
278	45	180	.41	-.40	.58	-.02
265	75	0	-.78	.24	-.82	.28
264	75	15	-.78	.24	-.82	.28
263	75	30	-.81	.25	-.85	.28
262	75	45	-.85	.27	-.89	.33
261	75	60	-.69	.23	-.73	.32
260	75	75	-.28	.10	-.30	.15
259	75	90	-.04	.02	-.04	.01
258	75	105	.16	-.03	.17	-.04
257	75	120	.46	-.10	.47	-.10
256	75	135	.68	-.18	.70	-.17
255	75	150	.65	-.17	.67	-.19
254	75	165	.68	-.18	.70	-.19
253	75	180	.70	-.21	.73	-.21

DATA FOR FILE: S22420

SINGLE STANDARD ARRAY - BL2, SCALE 1:24, H = 2 FT, P = 0

RUN #	BETA	WIND	CFX	CFY	CN	CMZ
165	25	0	-.20	.39	-.44	.08
163	25	135	.10	-.17	.20	.03
162	25	180	.13	-.25	.28	-.01
190	35	0	-.28	.38	-.47	.08
189	35	15	-.28	.38	-.48	.07
188	35	30	-.29	.41	-.50	.09
187	35	45	-.25	.38	-.46	.13
186	35	60	-.15	.26	-.30	.13
185	35	75	-.05	.10	-.11	.10
184	35	90	-.02	.02	-.03	-.03
183	35	105	.01	-.05	.05	-.06
182	35	120	.10	-.15	.18	-.03
181	35	135	.15	-.23	.27	-.04
180	35	150	.19	-.27	.33	.02
179	35	165	.20	-.29	.35	-.05
178	35	180	.23	-.30	.38	.04
169	45	0	-.36	.36	-.51	.10
168	45	180	.29	-.31	.43	-.05

DATA FOR FILE: S32420

SINGLE STANDARD ARRAY - BL3, SCALE 1:24, H = 2 FT, P = 0

RUN #	BETA	WIND	CFX	CFY	CN	CMZ
681	25	0	.00	.56	-.51	.73
682	25	180	.04	-.20	.20	-.31
680	35	0	-.29	.47	-.55	.08
679	35	15	-.30	.45	-.54	.07
678	35	30	-.30	.49	-.57	.08
677	35	45	-.26	.45	-.51	.10
676	35	60	-.21	.36	-.42	.04
675	35	75	-.09	.21	-.22	.03
674	35	90	-.00	.12	-.10	.02
673	35	105	-.01	.04	-.04	-.05
672	35	120	.13	-.09	.15	.06
671	35	135	.19	-.16	.24	.04
670	35	150	.20	-.19	.27	.05
669	35	165	.22	-.23	.31	.00
668	35	180	.23	-.23	.32	.03
684	45	0	-.04	.44	-.34	1.16
683	45	180	.19	-.23	.30	-.43

DATA FOR FILE: S12400

SINGLE STANDARD ARRAY - BL1, SCALE 1:24, H = 0.5 FT, P = 0

RUN #	BETA	WIND	CFX	CFY	CN	CMZ
352	35	0	-.40	.53	-.66	.15
353	35	45	-.41	.67	-.78	.17

DATA FOR FILE: S12410

SINGLE STANDARD ARRAY - BL1, SCALE 1:24, H = 1 FT, P = 0

RUN #	BETA	WIND	CFX	CFY	CN	CMZ
368	35	0	-.40	.58	-.71	.11
367	35	15	-.43	.61	-.74	.10
366	35	30	-.44	.64	-.78	.10
365	35	45	-.46	.68	-.83	.11
364	35	60	-.29	.48	-.56	.16
363	35	75	-.14	.24	-.27	.03
362	35	90	-.03	.08	-.08	-.00
361	35	105	.08	-.04	.08	.04
360	35	120	.18	-.17	.24	.03
359	35	135	.25	-.27	.36	.02
357	35	150	.29	-.32	.43	.02
356	35	165	.31	-.34	.46	.02
355	35	180	.32	-.35	.47	.04

DATA FOR FILE: S12430

SINGLE STANDARD ARRAY - BL1, SCALE 1:24, H = 3 FT, P = 0

RUN #	WIND	BETA	CFX	CFY	CN	CMZ
385	0	35	-.48	.68	-.83	.10
384	45	35	-.46	.77	-.89	.29

DATA FOR FILE: S12440

SINGLE STANDARD ARRAY - BL1, SCALE 1:24, H = 4 FT, P = 0

RUN #	WIND	BETA	CFX	CFY	CN	CMZ
381	0	35	-.49	.70	-.85	.13
380	15	35	-.51	.73	-.88	.13
379	30	35	-.54	.81	-.97	.16
378	45	35	-.50	.77	-.92	.21
377	60	35	-.31	.51	-.60	.17
376	75	35	-.13	.21	-.25	.03
375	90	35	-.04	.08	-.08	-.02
374	105	35	.06	-.02	.05	.04
373	120	35	.21	-.24	.32	.10
372	135	35	.35	-.45	.57	.08
371	150	35	.40	-.50	.64	.08
370	165	35	.39	-.49	.63	.03
369	180	35	.39	-.48	.62	.06

DATA FOR FILE: S12450

SINGLE STANDARD ARRAY - BL1, SCALE 1:24, H = 5 FT, P = 0

RUN #	WIND	BETA	CFX	CFY	CN	CMZ
345	0	35	-.52	.72	-.89	.12
346	45	35	-.49	.79	-.93	.33

DATA FOR FILE: A12420

ASPECT RATIO 2 (8 x 16 FT) - BL1, SCALE 1:24, H = 2 FT, P = 0

RUN #	WIND	BETA	CFX	CFY	CN	CMZ
397	15	35	-.39	.56	-.68	.15
396	30	35	-.39	.63	-.74	.27
395	45	35	-.38	.63	-.73	.23
394	60	35	-.25	.42	-.49	.11
393	75	35	-.08	.18	-.20	.08
392	90	35	-.00	.05	-.04	.03
391	105	35	.09	-.03	.08	.08
390	120	35	.21	-.22	.30	.09
389	135	35	.30	-.34	.45	.07
388	150	35	.36	-.41	.54	.13
387	165	35	.36	-.43	.56	.06
386	180	35	.35	-.44	.56	.04

DATA FOR FILE: B12420

ASPECT RATIO 4 (8 x 32 FT) - BL1, SCALE 1:24, H = 2 FT, P = 0

RUN #	WIND	BETA	CFX	CFY	CN	CMZ
437	0	35	-.41	.55	-.69	.08
438	15	35	-.42	.56	-.70	.06
439	30	35	-.41	.60	-.73	.11
440	45	35	-.37	.59	-.70	.15
441	60	35	-.24	.41	-.47	.11
442	75	35	-.09	.17	-.19	.03
443	90	35	-.00	.04	-.03	.02
444	105	35	.07	-.05	.08	.01
445	120	35	.19	-.19	.26	.04
446	135	35	.26	-.28	.38	.05
447	150	35	.30	-.32	.44	.06
448	165	35	.32	-.35	.47	.05
449	180	35	.34	-.36	.49	.07

DATA FOR FILE: D12421

POROUS ARRAY - BL1, SCALE 1:24, H = 2 FT, P = 2.5%

RUN #	WIND	BETA	CFX	CFY	CN	CMZ
644	0	35	-.45	.60	-.75	.06
645	30	35	-.46	.67	-.81	.09
646	45	35	-.42	.67	-.79	.17
647	60	35	-.27	.50	-.56	.17
648	120	35	.21	-.17	.26	.07
649	150	35	.31	-.34	.46	.04
650	180	35	.32	-.38	.49	.04

DATA FOR FILE: D12422

POROUS ARRAY - BL1, SCALE 1:24, H = 2 FT, P = 5%

RUN #	WIND	BETA	CFX	CFY	CN	CMZ
657	0	35	-.42	.60	-.73	.13
656	30	35	-.42	.62	-.75	.15
655	45	35	-.42	.64	-.77	.15
654	60	35	-.27	.49	-.56	.15
653	120	35	.15	-.17	.22	-.00
652	150	35	.29	-.33	.43	.02
651	180	35	.33	-.36	.48	.06

DATA FOR FILE: D12423

POROUS ARRAY - BL1, SCALE 1:24, H = 2 FT, P = 10%

RUN #	WIND	BETA	CFX	CFY	CN	CMZ
658	0	35	-.41	.58	-.72	.13
659	30	35	-.41	.61	-.73	.14
660	45	35	-.38	.60	-.71	.15
661	60	35	-.27	.45	-.53	.07
662	120	35	.19	-.15	.23	.03
663	150	35	.30	-.30	.42	.03
664	180	35	.35	-.37	.50	.06

DATA IN F FILES - BL1, SCALE 1:24, H = 2 FT

DATA FOR FILE: F21550

STANDARD ARRAY WITH FENCE - FP = 30%, LF = 15 FT, HF = 5 FT

RUN #	WIND	BETA	CFX	CFY	CN	CMZ
422	45	35	-.24	.33	-.40	.06

DATA FOR FILE: F22050

STANDARD ARRAY WITH FENCE - FP = 30%, LF = 20 FT, HF = 5 FT

RUN #	WIND	BETA	CFX	CFY	CN	CMZ
416	0	35	-.09	.10	-.13	.03
421	45	35	-.25	.38	-.45	.26

DATA FOR FILE: F23050

STANDARD ARRAY WITH FENCE - FP = 30%, LF = 30 FT, HF = 5 FT

RUN #	WIND	BETA	CFX	CFY	CN	CMZ
417	0	35	-.11	.11	-.15	-.03
420	45	35	-.32	.49	-.59	.14

DATA FOR FILE: F24050

STANDARD ARRAY WITH FENCE - FP = 30%, LF = 40 FT, HF = 5 FT

RUN #	WIND	BETA	CFX	CFY	CN	CMZ
418	0	35	-.13	.16	-.21	.00
419	45	35	-.41	.62	-.74	.15

DATA FOR FILE: F22020

STANDARD ARRAY WITH FENCE - FP = 30%, LF = 20 FT, HF = 2 FT

RUN #	WIND	BETA	CFX	CFY	CN	CMZ
431	0	35	-.30	.37	-.48	.06
423	45	35	-.41	.62	-.74	.16

DATA FOR FILE: F22040

STANDARD ARRAY WITH FENCE - FP = 30%, LF = 20 FT, HF = 4 FT

RUN #	WIND	BETA	CFX	CFY	CN	CMZ
430	0	35	-.12	.15	-.20	.04
424	45	35	-.32	.45	-.55	.16

DATA FOR FILE: F22060

STANDARD ARRAY WITH FENCE - FP = 30%, LF = 20 FT, HF = 6 FT

RUN #	WIND	BETA	CFX	CFY	CN	CMZ
429	0	35	-.04	.08	-.09	.02
425	45	35	-.20	.31	-.37	.11

DATA FOR FILE: F22080

STANDARD ARRAY WITH FENCE - FP = 30%, LF = 20 FT, HF = 8 FT

RUN #	WIND	BETA	CFX	CFY	CN	CMZ
428	0	35	-.02	.07	-.07	.06
426	45	35	-.11	.20	-.23	.07

DATA FOR FILE: F12050

STANDARD ARRAY WITH FENCE - FP = 0, LF = 20 FT, HF = 5 FT

RUN #	WIND	BETA	CFX	CFY	CN	CMZ
432	0	35	.04	-.01	.03	.00
433	45	35	-.27	.43	-.51	.14

DATA FOR FILE: F32050

STANDARD ARRAY WITH FENCE - FP = 50%, LF = 20 FT, HF = 5 FT

RUN #	WIND	BETA	CFX	CFY	CN	CMZ
435	0	35	-.17	.24	-.29	.01
434	45	35	-.25	.39	-.46	.15

DATA FOR FILE: F22055

POROUS ARRAY WITH FENCE - FP = 30%, LF = 20 FT, HF = 5 FT, P = 5%

RUN #	WIND	BETA	CFX	CFY	CN	CMZ
452	0	35	-.04	.09	-.10	.08
453	45	35	-.26	.37	-.45	.08

DATA FOR FILE: F22045

POROUS ARRAY WITH FENCE - FP = 30%, LF = 20 FT, HF = 4 FT, P = 5%

RUN #	WIND	BETA	CFX	CFY	CN	CMZ
451	0	35	-.12	.14	-.18	.02
454	45	35	-.30	.44	-.54	.12

DATA FOR FILE: F22025

POROUS ARRAY WITH FENCE - FP = 30%, LF = 20 FT, HF = 2 FT, P = 5%

RUN #	WIND	BETA	CFX	CFY	CN	CMZ
450	0	35	-.31	.37	-.48	.01
455	45	35	-.38	.57	-.69	.15

DATA FOR FILE: NE1F30

ARRAY FIELD,* UNIT NE1 - FP = 30%

RUN #	WIND	BETA	CFX	CFY	CN	CMZ
695	0	35	-.09	.13	-.15	-.01
699	30	35	-.06	.11	-.13	.04
700	45	35	-.18	.28	-.33	.07
701	60	35	-.19	.30	-.35	.09
847	135	35	.11	-.11	.15	.02

*All array field data have BL1, scale 1:24, H = 2 ft, LF = 20 ft, HF = 5 ft.

DATA FOR FILE: NE1F00

ARRAY FIELD, UNIT NE1 - FP = 0 (SOLID FENCE)

RUN #	WIND	BETA	CFX	CFY	CN	CMZ
704	0	35	.03	-.01	.03	.01
705	30	35	.03	-.03	.04	.02
706	45	35	-.15	.23	-.27	.10

DATA FOR FILE: NE1000

ARRAY FIELD, UNIT NE1 - NO FENCE

RUN #	WIND	BETA	CFX	CFY	CN	CMZ
709	0	35	-.42	.64	-.77	.12
708	30	35	-.50	.76	-.91	.10
707	45	35	-.43	.71	-.83	.20
848	315	35	.30	-.31	.43	.13

DATA FOR FILE: NE1S30

ARRAY FIELD, UNIT NE1 - SPECIAL CORNER FENCE; FP = 30%

RUN #	WIND	BETA	CFX	CFY	CN	CMZ
696	30	35	-.08	.11	-.13	.01
697	45	35	-.10	.15	-.17	.06
698	60	35	-.10	.15	-.18	.02

DATA FOR FILE: SW1F30

ARRAY FIELD, UNIT SW1 - FP = 30%

RUN #	WIND	BETA	CFX	CFY	CN	CMZ
731	135	35	.01	-.01	.02	.02
732	180	35	.05	-.10	.11	.00
733	210	35	.11	-.12	.16	-.03
734	225	35	.15	-.16	.22	-.03
735	240	35	.20	-.18	.27	.04
846	315	35	-.10	.15	-.18	-.05

DATA FOR FILE: SW1F00

ARRAY FIELD, UNIT SW1 - FP = 0 (SOLID FENCE)

RUN #	WIND	BETA	CFX	CFY	CN	CMZ
730	135	35	-.05	.11	-.11	.00
729	180	35	-.05	.16	-.16	.01
728	210	35	.01	-.07	.06	-.06
726	225	35	.24	-.40	.47	.00

DATA FOR FILE: SW1000

ARRAY FIELD, UNIT SW1 - NO FENCE

RUN #	WIND	BETA	CFX	CFY	CN	CMZ
722	135	35	.17	-.19	.25	.05
723	180	35	.35	-.49	.61	.08
724	210	35	.37	-.50	.62	.04
725	225	35	.33	-.39	.51	.08
845	315	35	-.34	.56	-.65	.08

DATA FOR FILE: SW1S30

ARRAY FIELD, UNIT SW1 - SPECIAL CORNER FENCE, FP = 30%

RUN #	WIND	BETA	CFX	CFY	CN	CMZ
739	210	35	.11	-.05	.10	-.00
737	225	35	.13	-.19	.23	-.02
736	240	35	.16	-.09	.17	.00

DATA FOR FILE: NE2F30

ARRAY FIELD, UNIT NE2 - FP = 30%

RUN #	WIND	BETA	CFX	CFY	CN	CMZ
843	0	35	-.10	.16	-.19	-.01
842	30	35	-.09	.14	-.17	-.06
841	45	35	-.06	.11	-.12	-.05

DATA FOR FILE: NE2F00

ARRAY FIELD, UNIT NE2 - FP = 0 (SOLID FENCE)

RUN #	WIND	BETA	CFX	CFY	CN	CMZ
838	0	35	.01	.01	-.02	-.05
839	30	35	-.02	.04	-.05	-.06
840	45	35	.03	.02	.04	-.01

DATA FOR FILE: NE2000

ARRAY FIELD, UNIT NE2 - NO FENCE

RUN #	WIND	BETA	CFX	CFY	CN	CMZ
826	0	35	-.40	.58	-.71	.08
827	30	35	-.34	.49	-.59	.07
828	45	35	-.26	.38	-.46	.00

DATA FOR FILE: SW2F30

ARRAY FIELD, UNIT SW2 - FP = 30%

RUN #	WIND	BETA	CFX	CFY	CN	CMZ
832	180	35	.08	-.06	.10	.04
833	210	35	.05	-.02	.05	.01
834	225	35	.02	.02	-.03	.00

DATA FOR FILE: SW2F00

ARRAY FIELD, UNIT SW2 - FP = 0 (SOLID FENCE)

RUN #	WIND	BETA	CFX	CFY	CN	CMZ
837	180	35	-.07	.14	-.16	.01
836	210	35	-.06	.13	-.14	.02
835	225	35	-.06	.16	-.17	.07

DATA FOR FILE: SW2000

ARRAY FIELD, UNIT SW2 - NO FENCE

RUN #	WIND	BETA	CFX	CFY	CN	CMZ
831	180	35	.37	-.47	.59	.06
830	210	35	.32	-.40	.51	.09
829	225	35	.24	-.26	.35	.14

DATA FOR FILE: NE3F30

ARRAY FIELD, UNIT NE3 - FP = 30%

RUN #	WIND	BETA	CFX	CFY	CN	CMZ
715	0	35	-.05	.09	-.10	.02
714	30	35	-.20	.30	-.36	.09
713	45	35	-.31	.47	-.56	.14
712	60	35	-.13	.21	-.25	.02

DATA FOR FILE: NE3F00

ARRAY FIELD, UNIT NE3 - FP = 0 (SOLID FENCE)

RUN #	WIND	BETA	CFX	CFY	CN	CMZ
711	30	35	-.23	.34	-.41	.03
710	45	35	-.37	.60	-.70	.19

DATA FOR FILE: NE3S30

ARRAY FIELD, UNIT NE3 - SPECIAL CORNER FENCE, FP = 30%

RUN #	WIND	BETA	CFX	CFY	CN	CMZ
716	30	35	-.15	.22	-.26	.04
717	45	35	-.19	.27	-.33	.03
718	60	35	-.08	.14	-.17	.02

DATA FOR FILE: SW3F30

ARRAY FIELD, UNIT SW3 - FP = 30%

RUN #	WIND	BETA	CFX	CFY	CN	CMZ
750	135	35	.01	.04	-.04	.02
748	180	35	.03	.05	-.06	.07
742	210	35	.16	-.10	.18	.09
743	225	35	.20	-.23	.30	.04
744	240	35	.13	-.13	.18	.05

DATA FOR FILE: SW3F00

ARRAY FIELD, UNIT SW3 - FP = 0 (SOLID FENCE)

RUN #	WIND	BETA	CFX	CFY	CN	CMZ
751	135	35	-.01	.07	-.07	.05
752	225	35	.26	-.34	.43	.05
753	240	35	.16	-.20	.25	.05

DATA FOR FILE: SW3S30

ARRAY FIELD, UNIT SW3 - SPECIAL CORNER FENCE, FP = 30%

RUN #	WIND	BETA	CFX	CFY	CN	CMZ
747	210	35	.10	-.10	.14	.01
746	225	35	.16	-.19	.25	.02
745	240	35	.12	-.11	.16	.06

DATA FOR FILE: NE4F30

ARRAY FIELD, UNIT NE4 - FP = 30%

RUN #	WIND	BETA	CFX	CFY	CN	CMZ
825	0	35	-.07	.12	-.13	-.03
824	30	35	-.05	.09	-.10	-.02
823	45	35	-.05	.08	-.09	-.06
822	60	35	-.05	.08	-.09	-.05

DATA FOR FILE: NE4000

ARRAY FIELD, UNIT NE4 - NO FENCE

RUN #	WIND	BETA	CFX	CFY	CN	CMZ
819	0	35	-.17	.26	-.31	-.10
820	30	35	-.18	.27	-.33	-.09
821	45	35	-.14	.24	-.27	.03

DATA FOR FILE: SW4F30

ARRAY FIELD, UNIT SW4 - FP = 30%

RUN #	WIND	BETA	CFX	CFY	CN	CMZ
812	180	35	.03	.04	-.05	.08
813	210	35	.03	.05	-.06	.13
814	225	35	.02	.03	-.04	.06
815	240	35	.01	.05	-.05	.05

DATA FOR FILE: SWF000

ARRAY FIELD, UNIT SW4 - NO FENCE

RUN #	WIND	BETA	CFX	CFY	CN	CMZ
818	180	35	.02	.07	-.07	.01
817	210	35	.01	.04	-.04	-.00
816	225	35	.03	.03	-.04	.04

DATA FOR FILE: NE5F30

ARRAY FIELD, UNIT NE5 - FP = 30%

RUN #	WIND	BETA	CFX	CFY	CN	CMZ
756	0	35	-.09	.13	-.16	-.05
757	45	35	-.17	.24	-.29	.00

DATA FOR FILE: SW5F30

ARRAY FIELD, UNIT SW5 - FP = 30%

RUN #	WIND	BETA	CFX	CFY	CN	CMZ
755	180	35	.06	-.00	.06	.12
754	225	35	.14	-.16	.21	-.05

DATA FOR FILE: NE6F30

ARRAY FIELD, UNIT NE6 - FP = 30%

RUN #	WIND	BETA	CFX	CFY	CN	CMZ
806	0	35	-.06	.10	-.11	.00
805	45	35	-.10	.14	-.17	.03

DATA FOR FILE: NE6F00

ARRAY FIELD, UNIT NE6 - FP = 0 (SOLID FENCE)

RUN #	WIND	BETA	CFX	CFY	CN	CMZ
807	0	35	-.07	.10	-.13	-.00
804	45	35	-.11	.15	-.18	.00

DATA FOR FILE: SW6F30

ARRAY FIELD, UNIT SW6 - FP = 30%

RUN #	WIND	BETA	CFX	CFY	CN	CMZ
809	180	35	-.00	.03	-.03	-.00
802	225	35	.03	-.00	.03	-.01

DATA FOR FILE: SW6F00

ARRAY FIELD, UNIT SW6 - FP = 0 (SOLID FENCE)

RUN #	WIND	BETA	CFX	CFY	CN	CMZ
808	180	35	.01	.02	-.02	-.00
803	225	35	.01	.01	.02	-.01

DATA FOR FILE: NE7F30

ARRAY FIELD, UNIT NE7 - FP = 30%

RUN #	WIND	BETA	CFX	CFY	CN	CMZ
778	0	35	-.13	.18	-.22	-.04
762	45	35	-.14	.17	-.22	-.03

DATA FOR FILE: NE730X

ARRAY FIELD, UNIT NE7 - FP = 30%, FIELD ROW 6 REMOVED

RUN #	WIND	BETA	CFX	CFY	CN	CMZ
777	0	35	-.15	.22	-.26	.01
761	45	35	-.13	.20	-.24	.04

DATA FOR FILE: NE7F00

ARRAY FIELD, UNIT NE7 - FP = 0 (SOLID FENCE)

RUN #	WIND	BETA	CFX	CFY	CN	CMZ
779	0	35	-.13	.19	-.23	-.01
763	45	35	-.11	.16	-.20	-.02

DATA FOR FILE: SW7F30

ARRAY FIELD, UNIT SW7 - FP = 30%

RUN #	WIND	BETA	CFX	CFY	CN	CMZ
774	180	35	.06	-.03	.06	.04
769	225	35	.16	-.12	.20	.32

DATA FOR FILE: SW730X

ARRAY FIELD, UNIT SW7 - FP = 30%, FIELD ROW 6 REMOVED

RUN #	WIND	BETA	CFX	CFY	CN	CMZ
775	180	35	.12	-.11	.16	.06
768	225	35	.17	-.22	.28	.05

DATA FOR FILE: SW7F00

ARRAY FIELD, UNIT SW7 - FP = 0 (SOLID FENCE)

RUN #	WIND	BETA	CFX	CFY	CN	CMZ
772	360	35	.05	-.04	.06	.00
770	405	35	.10	-.09	.13	-.03

DATA FOR FILE: NE8F30

ARRAY FIELD, UNIT NE8 - FP = 30%

RUN #	WIND	BETA	CFX	CFY	CN	CMZ
782	0	35	-.09	.15	-.18	.01
797	45	35	-.15	.22	-.27	.06

DATA FOR FILE: NE8F00

ARRAY FIELD, UNIT NE8 - FP = 0 (SOLID FENCES)

RUN #	WIND	BETA	CFX	CFY	CN	CMZ
781	0	35	-.09	.17	-.19	.05
798	45	35	-.21	.30	-.37	.06

DATA FOR FILE: NE83XX

ARRAY FIELD, UNIT NE8 - FP = 30%, FIELD ROWS 8, 9 REMOVED

RUN #	WIND	BETA	CFX	CFY	CN	CMZ
784	0	35	-.12	.18	-.22	-.03
795	45	35	-.18	.27	-.33	.05

DATA FOR FILE: NE830X

ARRAY FIELD, UNIT NE8 - FP = 30%, FIELD ROW 6 REMOVED

RUN #	WIND	BETA	CFX	CFY	CN	CMZ
783	0	35	-.13	.19	-.23	-.03
796	45	35	-.24	.34	-.41	.04

DATA FOR FILE: SW8F30

ARRAY FIELD, UNIT SW8 - FP = 30%

RUN #	WIND	BETA	CFX	CFY	CN	CMZ
790	180	35	.01	.02	-.02	-.00
792	225	35	.03	-.04	.05	-.05

DATA FOR FILE: SW8F00

ARRAY FIELD, UNIT SW8 - FP = 0 (SOLID FENCE)

RUN #	WIND	BETA	CFX	CFY	CN	CMZ
791	180	35	.02	.01	-.00	.01
799	225	35	.08	-.11	.14	-.04

DATA FOR FILE: SW83XX

ARRAY FIELD, UNIT SW8 - FP = 30%, FIELD ROWS 8, 9 REMOVED

RUN #	WIND	BETA	CFX	CFY	CN	CMZ
786	180	35	.02	.00	.01	-.01
794	225	35	.12	-.15	.19	-.02

DATA FOR FILE: SW830X

ARRAY FIELD, UNIT SW8 - FP = 30%, FIELD ROW 6 REMOVED

RUN #	WIND	BETA	CFX	CFY	CN	CMZ
787	180	35	.05	-.05	.07	-.01
793	225	35	.19	-.26	.32	.06